Journal of Materials Chemistry C

ROYAL SOCIETY OF CHEMISTRY

REVIEW

View Article Online
View Journal | View Issue

Cite this: J. Mater. Chem. C, 2022, 10, 13590

Understanding and minimizing non-radiative recombination losses in perovskite light-emitting diodes

Huiyuan Cheng,†[abc] Yaomiao Feng,†[abc] Yu Fu,[bd] Yifan Zheng,[ce] Yuchuan Shao*[ce] and Yang Bai*[abd]

Received 6th May 2022,
Accepted 13th July 2022

DOI: 10.1039/d2tc01869a

rsc.li/materials-c

Light-emitting diodes (LEDs) based on metal halide perovskites have shown great promise for next-generation display technology as they offer high color purity, satisfy Rec. 2020, and have low-cost solution processability. Moreover, metal halide perovskites exhibit extraordinary optoelectronic properties such as high photoluminescence quantum yields (PLQYs), feasible spectral tunability, narrow emission and high charge-carrier mobility, which has led to a rapid increase in the external quantum efficiencies (EQEs) of up to 28% for perovskite light-emitting diodes (PeLEDs) over the past few years. Nevertheless, further increase in efficiency is impeded in these state-of-the-art devices due to the presence of non-radiative recombination losses, which also limits their operational stability. In this review, we provide a fundamental analysis of the predominant pathways that induce non-radiative recombination losses in PeLEDs, followed by a discussion on what and how reliable characterization techniques could be used to evaluate such losses. We also summarize and critically assess the most recent advances in suppressing non-radiative recombination in PeLEDs. Finally, we discuss the remaining challenges and outline future directions that aim to minimize non-radiative recombination losses and boost the efficiency of PeLEDs towards their radiative limit.

[a] Australian Institute for Bioengineering and Nanotechnology, The University of Queensland, Brisbane, St Lucia, Queensland 4072, Australia. E-mail: y.bai@uq.edu.au
[b] Faculty of Materials Science and Engineering/Institute of Technology for Carbon Neutrality, Shenzhen Institute of Advanced Technology, Chinese Academy of Sciences, Shenzhen 518055, China. E-mail: y.bai@siat.ac.cn
[c] Key Laboratory of Materials for High-Power Laser, Shanghai Institute of Optics and Fine Mechanics, Chinese Academy of Sciences, Shanghai 201800, China. E-mail: shaoyuchuan@siom.ac.cn
[d] Shenzhen Key Laboratory of Energy Materials for Carbon Neutrality, Shenzhen 518055, China
[e] School of Physics and Optoelectronic Engineering, Hangzhou Institute for Advanced Study, UCAS, Hangzhou 310024, China
† These authors contributed equally.

Huiyuan Cheng

Huiyuan Cheng is a PhD candidate at The University of Queensland (UQ), Australia. She is also a visiting student on a joint program funded by Chinese Academy of Sciences and UQ. She obtained her Master's degree from the University of Science and Technology of China (USTC). Her research interest is focusing on metal halide perovskite nanocrystal light-emitting diodes.

Yaomiao Feng

Yaomiao Feng is now a PhD candidate at The University of Queensland (UQ), and also a visiting student on a joint program funded by Chinese Academy of Sciences and UQ. He received his Master Degree in Applied Chemistry from the Shanghai Normal University and then became a Research Assistant in Department of Chemistry, Southern University of Science and Technology. His research interest lies in the design and synthesis of novel inorganic/organic hybrid perovskite materials for optoelectronic devices.

1. Introduction

Metal halide perovskites, which have achieved incredible success in photovoltaics, have also gained considerable attention as an emerging class of emitter materials for next-generation lighting and display technologies. This is because perovskite emitters have shown superiority in many aspects, such as ease of solution processability, narrow emission, wide colour gamut that meets the requirement of Rec. 2020 standard for ultra-high-definition displays, feasible spectral tunability, near-unity photoluminescence quantum yields (PLQYs), and high charge-carrier mobility, outperforming other emitters used in commercial products.[1,2] Thanks to these extraordinary properties as well as the lessons learnt from other LED technologies, *i.e.*, organic LEDs (OLEDs) and quantum dot LEDs (QLEDs), the past few years have witnessed a tremendous rise in electroluminescence efficiency of perovskite LEDs (PeLEDs), with the external quantum efficiency (EQE) skyrocketed from 0.1%[3] to 28.1%.[4]

Despite such impressive advances, the electroluminescence performance of PeLEDs, particularly blue PeLEDs, still lags behind those of commercial LED devices, such as OLEDs.[5] One of the key reasons is that the presence of non-radiative recombination is still prominent in PeLEDs, which impedes further efficiency enhancement.[6,7] The predominant pathways that induce non-radiative recombination losses mainly include trap-assisted recombination, Auger recombination and interface-induced recombination.[6]

Unlike the perovskite films for photovoltaic application, the emissive perovskite films employed in LEDs need to be very thin (several ten nanometres) and are usually comprised of considerably smaller sized polycrystals or nanocrystals, which aims to spatially confine the charge carriers and increase the radiative bimolecular recombination rates in the emitter layers. Nevertheless, this results in significantly increased surface area-to-volume ratio and larger density of defects in perovskite emitters.[8,9] Several types of point defects such as halide and A-site vacancies, Pb-halide anti-sites and iodine interstitials as well as the defects at the device interfaces[7] have proven to be associated with trap states that induce the trap-assisted non-radiative recombination,[2,10,11] which is the key reason for the luminous efficiency loss at relatively low charge-carrier densities. While Auger recombination becomes dominant in PeLEDs at higher charge-carrier densities causing efficiency roll-off, despite that three-dimensional perovskites have been demonstrated to be promising for high-brightness LEDs.[12] In addition, the non-optimal energy level alignment together with unbalanced charge injection within PeLEDs leads to carrier accumulation at the interfaces, which increases the probability of Auger recombination and deteriorate the device performance.[13–16] Furthermore, the presence of abundant defects and non-radiative recombination in PeLEDs will also impair their operational stability. The defects, acting as ionic shuttles, were shown to boost the migration of ions such as halides and thus cause the shift of emission wavelength, which reduce the color purity and long-term spectra stability of PeLEDs.[17,18] Non-radiative recombination, particularly Auger recombination, generate significant amount of Joule heat, which also accelerates the device degradation.[19,20]

Therefore, the control of non-radiative recombination processes in PeLEDs is crucial for achieving high electroluminescence performance and stability. Tremendous efforts have recently been devoted to exploring effective strategies for suppressing non-radiative recombination losses in PeLEDs, including crystal size manipulation,[21–24] exciton binding energy tuning,[25,26] defect passivation,[27,28] interface engineering,[29,30] and so forth. Yet there remains a significant gap in terms of the luminous efficiency and device lifetime to meet the requirements of commercialization. It is thus in urgent need of a systematic and in-depth overview focusing on the understanding and latest advances in the mitigation of non-radiative recombination in PeLEDs, which serves as a guide for their further development towards practical applications.

Yuchuan Shao

Yuchuan Shao received his BS Degree from the University of Science and Technology of China (USTC) in 2009. He completed his Master's Degree in Shanghai Institute of Optics and Fine Mechanics (SIOM) in 2012 and his PhD Degree from the University of Nebraska–Lincoln. After a postdoc period at Yale University and University of North Carolina at Chapel Hill, in 2019, he joined SIOM as a Professor of photoelectronics. His current research interest focuses on perovskite optoelectronic devices.

Yang Bai

Yang Bai is currently an Associate Professor at Shenzhen Institute of Advanced Technology (SIAT), Chinese Academy of Sciences and also an Honorary Senior Research Fellow at The University of Queensland (UQ), Australia. Yang received his PhD in Chemical Engineering from UQ in 2014, and then he moved to the United States to conduct a two-year postdoc training at the University of Nebraska-Lincoln. Before joining SIAT, he has worked at UQ for four years. Bai's research focuses on the design and synthesis of hybrid semiconductor materials for new-generation thin film photovoltaics and optoelectronics.

In this review, we first present a fundamental understanding of the origin and nature of the non-radiative recombination losses in PeLEDs, which mainly covers the trap-assisted recombination, Auger recombination and interface-induced non-radiative recombination. Then, advanced characterization techniques used to quantify these non-radiative recombination losses in PeLEDs are discussed, and recent advances in suppressing such losses are also critically assessed. Finally, we give our perspectives on future work that potentially could minimize non-radiative recombination losses and further improve the luminous efficiency and stability of PeLEDs to meet the needs of commercialization.

2. Fundamentals of PeLEDs

2.1 Electroluminescence efficiency

EQE is one of the key parameters used to evaluate the efficiency of PeLEDs, defining as the ratio of photons escaping from the device to the charge carriers across the device. In general, there are four factors that must be optimized to maximize the EQE of the PeLED device:[31]

(i) Charge carrier balance. The ratio of electrons and holes injected into emitter layer should be closed to 1.

(ii) Leakage current. Charge carriers across the device without forming a correlated electron–hole pairs should be minimized.

(iii) Recombination. Non-radiative recombination processes should be suppressed.

(iv) Light extraction. Outcoupling of generated photons from device to free area should be maximized.

Therefore, the EQE of the PeLEDs can be defined as[31]

$$\begin{aligned} \mathrm{EQE} &= \frac{\text{Number of photons escape from device}}{\text{Number of carrier across device}} \\ &= \eta_{\mathrm{inj}} \cdot \eta_{\mathrm{e-h}} \cdot \eta_{\mathrm{rad}} \cdot \eta_{\mathrm{out}} \end{aligned} \quad (1)$$

where η_{inj} is the carrier injection efficiency, representing the balance of carrier injection in the emitter layer; $\eta_{\mathrm{e-h}}$ is the excitons forming efficiency, representing the probability of forming an electron–hole pair to per pair of oppositely charged carriers injected; η_{rad} is the radiative recombination efficiency that is closely related to PLQY or internal quantum efficiency (IQE); and η_{out} is the outcoupling efficiency, meaning the ratio of photons escaping from diode to those generated in the emitter layer. Based on the above theory, we expect the EQE of PeLEDs would benefit from the combination of a high-quality perovskite emitter layer featuring low defect density, optimized charge transport layers offering balanced carrier injection, and a device structure enabling efficient photon extraction.

2.2 Charge carrier recombination

Charge carrier recombination is a process by which electrons and holes in the semiconductor are annihilated.[32] The applied bias drives a huge number of electrons and holes into the device, and charge carriers annihilate almost simultaneously due to electron–hole recombination. The recombination process can be classified as radiative and non-radiative recombination, as shown in Fig. 1(a–c). Photons are emitted from radiative processes, and they should be maximized to achieve high luminance. The electric energy is converted into other forms of energy, such as heat, rather than luminous energy in the non-radiative process, which degrades the device's performance and operational stability. The recombination process can be described as following:[33]

$$-\frac{\mathrm{d}n}{\mathrm{d}t} = k_1 n + k_2 n^2 + k_3 n^3 \quad (2)$$

where n represents the charge carrier concentration; k_1, k_2, and k_3 are the first-order, second-order and third-order rate constants associated with trap-assisted recombination, radiative recombination, and Auger recombination, respectively. The recombination rate constants can be determined by photoluminescence decay and pump–probe spectroscopy. Normally, k_1 can be experimentally determined from the kinetics at much longer decays with low pump fluence, under which higher order recombination contributions are negligible. k_2 and k_3 can be obtained from global fitting of the decay kinetics for different excitation fluences.

2.3 Non-radiative recombination pathways

The presence of non-radiative recombination is not conducive to obtaining high-efficiency and stable PeLEDs. Hence, it is crucial to understand the pathways and explore solutions to reduce and eliminate non-radiative recombination within the PeLEDs. In this review, the non-radiative recombination pathways are classified as trap-assisted recombination, Auger recombination and interface-induce recombination.

Trap-assisted recombination, also known as Shockley–Read–Hall (SRH) recombination (Fig. 1(b)), is a two-step transition *via* a defect within the band gap.[34] Firstly, an electron (or a hole) is trapped by an energy state in the forbidden region which is introduced through defects in the crystal lattice. Then, if a hole (or an electron) moves up to the same energy state before the electron is thermally re-emitted into the conduction band, the trap-assisted recombination occurs. The trap-assisted non-radiative recombination discussed here refer to that induced only by the bulk or surface defects of perovskite emitter layer including polycrystalline thin films and colloidal nanocrystals.

Similar to conventional semiconductors, the typical defects in perovskite can be classified as point defects (including vacancies, interstitials, anti-sites) and structural defects (including dislocations, grain boundaries).[35] Defects can cause trap states near the band edge (shallow defects) or within the bandgap (deep defects) to capture charge carriers. Among conceivable defects, interstitial and anti-site defects can form deep trap states in the electronic structure. Deep trap is the main pathway for the loss of charge carriers and non-radiative recombination in perovskite materials.[10] However, these defects are normally absence in the perovskite lattice since they have high formation energies.[36] Only vacancy defects with sufficiently low formation energies are exclusively observed.[9] Fortunately,

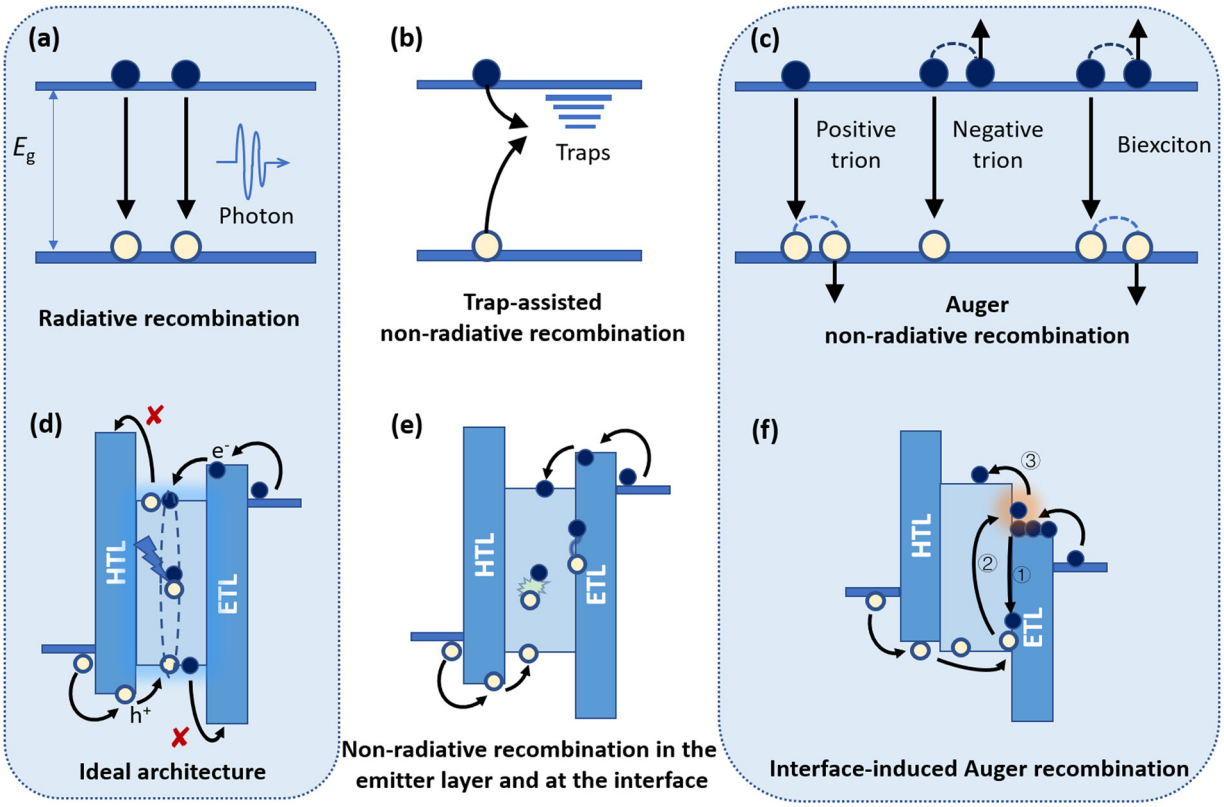

Fig. 1 (a–c) Charge carrier recombination mechanism in perovskite, including radiative recombination (a) trap-assisted non-radiative recombination (b), and Auger non-radiative recombination (c). Diagrams showing the ideal PeLEDs architecture (d), origins of non-radiative recombination in the emitter layer and at the interface (e) and interface-induced Auger recombination (f).

these shallow defects usually occur on the surface and can be easily passivated by simple chemical modification, such as the use of ligands in nanocrystals and additives in polycrystalline film. Normally, the lattice parameter decreases with halide changing from I^- to Br^- to Cl^- in metal halide perovskite. This leads to stronger interactions between Pb^{2+} dangling bonds when halide vacancies form, which gives rise to deeper trap level for the halide vacancy when combined with lower electron affinity. Thus, Cl-based perovskite are intended to form deep trap and low PLQY, while Br-based and I-based perovskite primarily form shallow traps and high PLQY.[35] Therefore, much attentions have been paid to decreasing the trap density and reducing non-radiative losses in recently years, which will be discussed further in the following sections.

Auger recombination is another unavoidable non-radiative recombination, during which the energy released by electron–hole recombination is transferred to other charge carrier, rather than being released as photons or heat energy.[37] Auger recombination is a multiexcitons decay process (Fig. 1(c)) and highly dependent on the density of charge carriers, which usually leads to significant photoluminescence quenching at high carrier concentration ($>10^{17}$ cm^{-3}).[20,38] The simplest charged state is a trion, which comprises a neutral exciton and either an extra hole (positive trion, X^+) or an extra electron (negative trion, X^-).[39] Meanwhile, Auger decay can also generate neutral multiexcitons such as biexcitons. All these Auger processes could cause non-radiative recombination and thus deteriorate the PLQY and PL lifetime, which have a paramount impact on the performance and stability of PeLEDs.

Reducing the Auger recombination is recognized as one of the primary approaches for improving PeLED performance at high carrier concentration. However, the Auger recombination rate of halide perovskites ($\approx 10^{-28}$ cm^6 s^{-1}) is much faster than that of traditional III–V (GaAs, $\approx 10^{-30}$ cm^6 s^{-1})[40] or II–VI (CdTe, $\approx 10^{-32}$ cm^6 s^{-1})[41] semiconductor. The unexpectedly strong Auger recombination rate in perovskite is attributed to a coincidental resonance of the bandgap with states that are roughly one bandgap away from the band edges.[42] The strong Coulomb interaction between the hole and electron leads to a non-uniform carrier distribution, because a carrier is more likely to be surrounded by the opposite charged carriers, which strengthens Auger recombination at the same position.[43,44] In addition, the distortions in metal-halide lattice affects the state distribution, and contributes significantly to the high Auger rate.[42] All these factors together contribute to ultra-strong Auger recombination in perovskite materials. In addition, unbalanced injection of electrons and holes at interfaces can cause Auger recombination, which will be described in the next section.

Interface-induced recombination is usually caused either by the presence of interfacial defects or the mismatched energy-level alignment among different layers. In an ideal case as

exhibited in Fig. 1(d), the perfect selective layers are expected to have a smooth morphology that leads to a defect-free interface with emitter layer, and in the meantime, allow either electrons or holes to be injected through while block the opposite charged carriers at the interface. Nevertheless, in reality, there are usually numerous defects at the interfaces between different layers, causing non-radiative recombination (Fig. 1(e)).[13,45] The formation of such interfacial defects is mostly correlated with the poor affinity of each layer at the interfaces, which increases the difficulties in film deposition and thus may lead to film discontinuity with pinholes.[46] Such interfacial defects not only exacerbate non-radiative recombination,[7,45] but also impose an adverse impact on the efficient injection of charge carriers.[47] The losses associated with interface-induced recombination could be mitigated by defect passivation and interfacial engineering.[31,46] In addition to the interface defects, the imbalanced injection of electrons and holes due to the non-optimal energy level alignment is another key issue that can cause interface-induced non-radiative recombination, particularly Auger recombination in PeLEDs.[48,49] Recent studies indicated that even a slight imbalance between electron and hole injection can lead to a serious efficiency roll-off.[6,50] A typical example is illustrated in Fig. 1(f), where there is an energy barrier present at the interface of electron transport layer (ETL) and emitter layer. Under a forward bias, the holes could pass through the interface of hole transport layer (HTL) and emitter layer easily since the energy barrier is negligible. The holes then accumulate at the ETL/emitter layer interface due to the presence of a large energy barrier in between. In the meantime, the injected electrons also accumulate at the interface of ETL and emitter layer due to emitter the presence of a significant energy barrier. The simultaneous accumulation of electrons and holes at the ETL/emitter layer interface facilitates the occurring of Auger recombination, which enables the third electrons with sufficiently high energy to inject into emitter layer and radiatively recombine with holes in the same layer.[48] This also applies to the situation where there is a considerable energy barrier at the HTL/emitter layer interface.[51] Therefore, device engineering is of paramount to suppress interface-induced recombination by achieving an optimal energy level alignment and balanced carrier injections.

3. Advanced characterizations for non-radiative recombination analysis

To unveil the mechanisms of non-radiative recombination in PeLEDs, a number of advanced characterization techniques have been employed to study the charge carrier dynamics and their correlations with the optoelectronic properties and device performance. In this section, we present a summary of the key techniques such as steady-state and transient spectroscopy, and discuss how these techniques are used to analyse the non-radiative losses caused by defect-assisted recombination, Auger recombination, and interface-induced recombination.

3.1 Steady-state spectroscopy

3.1.1 PL spectroscopy. Steady state PL is a foundational tool in investigating the luminescent property of perovskite. By simply comparing the PL intensity and wavelength before and after the passivation can reflect the metrics of radiative recombination.[7] The main peak in spectra normally reflect the directly band-to-band radiative recombination. If the emitter layers are modified with additives, the PL peak would slightly blue shift to shorter wavelength, accompanying with the decreasing in peak width, which suggests the reduction of shallow defects on the grain boundaries and surfaces.[52,53] Moreover, The broaden in peak width and shifted in wavelength can be observed in temperature-dependent PL method, which can provide useful information for material properties, such as charge carrier recombination and trapping channels in perovskite.[54] In general, the temperature-dependent PL data could be fitted by the Arrhenius model,

$$I(T) = \frac{I_0}{1 + A e^{-\frac{E_b}{k_B T}}} \quad (3)$$

where I_0 is the PL intensity at 0 K, A is the free parameter related to the trap state, k_B is the Boltzmann constant, and E_b is the excitons binding energy or effective activation energy. The E_b can be extracted from this equation, which affects the efficiency of charge transfer, exciton dissociation probability, and radiative recombination.

The non-radiative recombination can be suppressed at low temperature, as the traps are frozen out in such situation. The fluctuation concentration of defects may be responsible for reversible PL intensity loss with elevated temperatures. Therefore, E_b can represent the activation energy for charge carrier trapping.[55] If the fitted trapping activation energy matches the non-radiative recombination defect energy level, it can reflect the behaviour of this defect thermal quenching in emission.[55,56] By fitting the reversible PL loss of the $CsPbBr_3$ nanocrystals, the activation energy of Br vacancies defects can be obtained (246 meV), which is consistent with density functional theory (DFT) calculations.[55] The agreement between experimental data and calculated trap energies leads us to identify the mechanism of reversible PL loss in $CsPbBr_3$ nanocrystals as thermal electron occupation of halogen vacancy centers.[27] By passivating the nanocrystals with didodecyl dimethylammonium fluoride (DDAF), the activation energy for trapping value rose with the increasement of DDAF adding, indicating that the surface bromine vacancies are effectively passivated.[55] Moreover, it should be noted that the sub-bandgap and phase state often changes with the temperature transformation, owing to the fragile nature of perovskite. As shown in Fig. 2(a), band-tail PL emission dominates at very low temperatures and phase transition occurs at around 150 K. The trap energies and densities are slightly different in these phases, which also influence the charge carrier recombination process.[57,58] Explicit interpretation could be obtained when the analysis considers the phase transition or take into

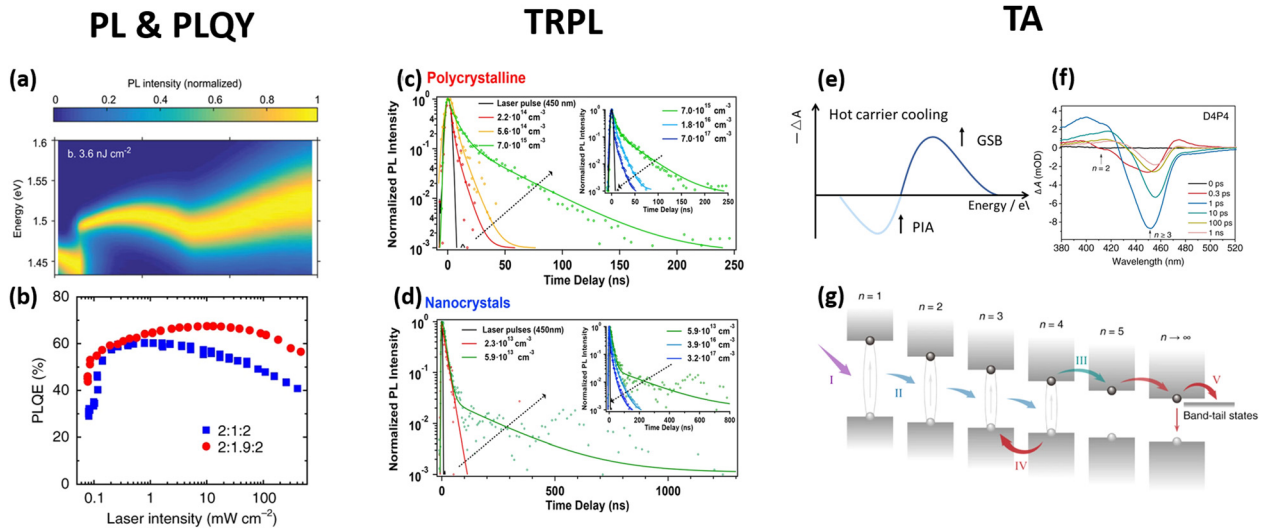

Fig. 2 (a) False-colour plot of PL spectra of $FA_{0.95}Cs_{0.05}PbI_3$ thin film at low fluence 3.6 nJ cm^{-2} as a function of temperature between 4 and 295 K. A phase transition occurs at 150 K. Reproduced with permission from ref. 54. Copyright © 2020, Wiley-VCH GmbH; (b) excitation-intensity-dependent PLQY of the multiple quantum wells perovskite films under continuous-wave laser excitation. Reproduced with permission from ref. 12. Copyright © 2018, The author(s), Springer Nature; (c) TRPL dynamics of polycrystalline perovskite, and (d) nanocrystals obtained at different excitation densities. The insets show the PL dynamics recorded at high excitation densities where the dependence of the lifetime on the excitation density is opposite than the one observed at low excitation densities. The arrows indicate an increase in the excitation density. Reproduced with permission from ref. 67. Copyright © 2018, American Chemical Society; (e) diagram illustrated the feature of TA spectra during the hot carrier cooling process. (f) TA spectra at different delay times for the quasi-2D perovskite film. (g) Schematic diagram of charge carrier behaviour after excitation. The carrier recombination progress can be divided into five stages: I, carrier formation; II, exciton transfer; III, charge transfer; IV, reverse charge transfer; V, continuous charge transfer and recombination. (f) and (g) were reproduced with permission from ref. 89. Copyright © 2020, The Author(s), Springer Nature.

consideration of charge-carrier dynamics in certain temperature regimes.[59]

3.1.2 PLQY measurement. PLQY is a key parameter to quantify non-radiative recombination losses, typically defined as the ratio of the number of emitted photons to the number of adsorbed photons. It can be calculated using

$$\mathrm{PLQY} = \frac{\text{the number of emitted photons}}{\text{the number of adsorbed photons}} = \frac{k_2 n}{k_1 + k_2 n + k_3 n^2} = \frac{1}{1 + \frac{k_1}{k_2 n} + \frac{k_3 n}{k_2}} \quad (4)$$

According to such equation, the PLQY is strongly related to n. (Fig. 2(b)) In the free carrier system, PLQY depends on the competition between trap-assisted non-radiative recombination and radiative recombination under low excitation intensity. When increasing the intensity, radiative bimolecular recombination gradually dominates over the charge carrier trapping. At even higher carrier density, where Auger recombination becomes effective and dominates over the bimolecular recombination, the PLQY then decreases dramatically.[12] Meanwhile, the PLQY is also depended on the coefficient of each recombination (k_1, k_2, k_3).[33] The maximum value of $\left(1 + 2\sqrt{k_1 k_3 / k_2^2}\right)^{-1}$ can be achieved at the carrier density is $\sqrt{k_1/k_3}$.[60] In addition, according to simulated results of the relationship between PLQY and coefficients of non-radiative recombination (k_1 and k_3), PLQY increases dramatically with the decrease of k_1 or k_3, indicating that the reduction of non-radiative recombination is an effective approach to improve PLQY.

The PLQY of different samples can be used to quantify the recombination losses in the bulk, at the interfaces, and/or metal contacts.[61] For instance, the PLQY of perovskite thin film increases from 12% to 78% after adding dual-additive (18-crown-6 and poly(ethylene glycol) methyl ether acrylate), which indicates the dual additives containing C–O–C bonds can suppress non-radiative recombination in the bulk of perovskite.[4,62] Moreover, the comparison of PLQY values between as-synthesized colloidal nanocrystals and as-deposited nanocrystal thin film could reflect the non-radiative loss caused by nanocrystal assembly.

In general, the PLQY depends on a few factors, including the quality of the perovskite polycrystalline film or nanocrystals, the value of E_b,[63] the efficiency energy transfer among different phases,[20] the energy level of transfer layers, and additional recombination pathways at the perovskite/transfer layers.

3.2 Transient spectroscopy

Because carrier transportation and recombination processes always accomplish within ultrafast timescales (from ps to ms), dynamical measurements related to optics and electricity are of interest to be taken into study. Moreover, the non-radiative transitions typically exhibit a much shorter lifetime than radiative recombination, indicating the requirement of transient techniques with higher time-resolution.[64] Therefore, transient characterizations become an indispensable tool for studying

the recombination mechanisms of charge carriers and/or excitons. Herein, we introduce two common transient measurements to observe charge carriers' behaviours.

3.2.1 Time-resolved photoluminescence (TRPL). TRPL, also called as transient photoluminescence, has been employed as a powerful tool to measure radiative electron–hole recombination after an excitation light pulse. The decay of the PL emission over time (Fig. 2(c and d)) can be fitted by the model multi-exponential function of[65,66]

$$I(t) = \sum_n A_n e^{-\frac{t}{\tau_n}} \quad n = 1, 2, 3, \ldots \tag{5}$$

where A_n, τ_n represents the amplitudes and delay time/lifetime of the nth component, respectively.

The average lifetime can be calculated as followed

$$\tau_{avg} = \frac{\sum_n A_n \tau_n^2}{\sum_n A_n \tau_n} \quad n = 1, 2, 3, \ldots \tag{6}$$

In case of neat perovskite film, the PL decays follow single exponential behaviour under sufficiently low excitation fluence, which has been assigned to a first-order loss process, such as trap-assisted recombination. The lifetime is relatively low in this situation because the trap-assisted non-radiative recombination is dominant. By increasing the fluences to a higher level, the saturation of trap states deactivates the non-radiative relaxation pathways, giving rise to an increase in PL at first. And then bimolecular radiative and Auger recombination enhance and successively become dominant in the PL dynamics. At high excitation density, the amplitude of these fast component increases, resulting in the decreasing of effective lifetime. Accordingly, multi-exponential fitting is applied to analyse the carrier dynamics under high excitation.[20] That is the reason why, as seen in the Fig. 2(c and d), the dynamic slows down at first and subsequently speeds up as the increasement of excitation density, both in polycrystalline and nanocrystals samples.[67]

Normally, the fast delay (A_1, τ_1) is related to trap-assisted recombination and the slow delay (A_2, τ_2) associates with the radiative recombination. The variation of these parameters before and after the modification of samples can reflect the behaviour of charge carrier recombination. The lessened A_1 indicates less trap-assisted recombination at grains' boundaries/interfaces or nanocrystals' surface, while increased A_2 manifests more radiative recombination inside the perovskite, ultimately contributing to electroluminescence efficiency.[66,68] Therefore, the longer lifetime indicates stronger radiative recombination, while the shorter lifetime related to the non-radiative recombination of trap capture or Auger process.[17] Normally, the faster PL decay time and lower PLQY in the case of chloride-based nanocrystals suggest that they exhibit higher non-radiative rates as compared to the iodide and bromine-based nanocrystals.[69,70] The mixed anion nanocrystals shows dynamics processes between two pure-anion perovskite.[71]

The TRPL can not only reflect the traps-assisted and Auger recombination, but it can also reflect the non-radiative loss at the interfaces.[15,72] By comparing the TRPL spectra of the perovskite with and without HTL/ETL, we can measure the non-radiative recombination events at the two contact interfaces. If the adding of charge-transport layers does not influence lifetime of carriers, it can indicate non-radiative recombination events at the two contact interfaces are insignificant.[62] For example, the TRPL of pure perovskite films with the polymer component (poly(2-hydroxyethyl methacrylate)) and such film on the CTL are almost the same, indicating the interfacial luminescence quenching processes are insignificant.

TRPL is a sensitive measurement for analysing the carriers' behaviour. But it is difficult to measure the process of exciton formation or decay to free-carrier dynamics, because the TRPL is sensitive to the presence of both free carriers and excitons.[73,74] Also, PL lifetime for each bandgap species (n = 1, 2, 3,...) in quasi-two-dimensional (quasi-2D) perovskite cannot extract from TRPL to illustrate energy transfer kinetics because of the limitation of this instrument.[75] Therefore, to analyse the carrier dynamic process in perovskites, TRPL should be combined with other precision measurements.

3.2.2 Transient absorption spectroscopy (TA). TA spectra records any change in the absorption spectrum as a function of time and wavelength, respectively categorized as transmission and reflection mode. With excellent in time resolution, TA can reflect the photoinduced change in absorption (ΔOD) as a function of the delay between a pump and a probe pulse, which can be distinguished as ground-state blenching (GSB), stimulated emission, and photoinduced absorption (PIA) of photogenerated charges.[64]

For perovskite nanocrystals, the early time ($\Delta t < \tau_{cool}$) TA spectra exhibit a typical trait of Coulomb-interaction-induced red shift of the band edge transition, whose shape look as an asymmetric derivative-like feature with PA at lower energies and GSB at higher as shown in Fig. 2(e).[71,76] This process is in order of sub ps or even fs, which is shorter than excitons cooling and exciton recombination.[31] After $\Delta t > \tau_{cool}$, the derivative feature in the TA spectra disappears due to state filling, in which PA signal eventually decays and a very strong band-edge bleaching signal occurs. Further, the charge carriers are located at the band-edge after hot-carrier cooling. During this time, Auger decay is domain over radiative recombination if a nanocrystal has more than one exciton.[77] After Auger processes, band to band radiative recombination and trap-assisted non-radiative recombination can occur simultaneously.[64] Hence, in order to observe different state of carrier dynamic process, the delay time of TA should be carefully determined. Tracking GSB peak after the carrier cooling process as function of time and fitting the data with the eqn (5) can get the information of the carrier recombination process. Consistent with the TRPL decay, the fast decay and long decay components are associated with non-radiative and radiative recombination, respectively. Normally, post treating the nanocrystal can prolong the long decay, which indicates the passivation of defects.[19]

For quasi-2D perovskite thin films, the peaks of species (n = 1, 2, 3,...) could be easily distinguished in TA spectrum (Fig. 2(f)), because the peak position of GSB peaks are in agreement with peaks in the steady-state absorption spectrum.[75,78] In general, several peaks can be identified in the spectra, suggesting the quasi-2D perovskite films are not single-phase, but a mixture of n values. If the major peak directly mirrors the lowest bandgap component in the steady-state PL spectrum, it might imply that photoexcitation transfer is occurring in these materials. Therefore, the TA spectra can reflect the process of cascade energy transfer from smaller-n phases to larger-n phases in quasi-2D perovskites (Fig. 2(g)),[75,79] or from quasi-2D to 3D phase perovskite in hybrid systems.[66]

Other transient characterization measurements based on frequency, such as terahertz photoconductivity spectra (THz), can also monitor charge carrier recombination in a sub-femtosecond timescale.[80] In addition, photoinduced time-resolved microwave conductivity (TRMC) can be applied as a complementary technique to probe charge carrier lifetimes.[81] Despite many theories that underpin these studies, the time delayed collection field aim to identify the carrier dynamic process after the excitation pulse, which can provide fundamental information of radiative and non-radiative recombination.

3.3 Other optical and electrical measurements

As the non-radiative recombination can directly weaken the PL intensity, PL related methods are extensively used in this field. Beside the optical measurements mentioned above, the losses can be visualized by considering the microscale PL mapping. Normally, the non-radiative recombination sites in the emitter film are randomly distributed. The PL intensity heterogeneities indicate that PL quenching sites are likely formed at the ends of the nanocrystals where the chemical or structural defect formation is most probable.[82] Moreover, combining with time resolution, PL blinking can be observed.[83] This phenomenon most probably caused by charge trapping at surface states,[84] or the Auger recombination between photogenerated electron–hole pairs and charges captured by electronic trap sites.[85]

Apart from the methods mentioned above, other electrical ways used in QLEDs and PSCs can also be applied to PeLEDs. Among these methods, space charge limited current (SCLC) has been widely used in probing the trap density and carrier mobility in perovskite.[75,86] This measurement records the current density with varying the applied voltage in the hole-only or electron-only device. The trap density can be calculated from the lower value of trap-filled limit voltage (V_{TFL}). Thermal admittance spectroscopy (TAS)[87] is another widely used technique to quantify the trap density of state (tDOS) by measuring the device capacitance and conductance as a function of frequency and temperature. Additionally, it could provide an energy level profile of different traps. Time-resolved transient electroluminescence (TREL)[88] has been widely used in QLEDs to investigate the pertinent kinetic processes in operational devices. This method can also be utilized in understanding the dynamics in operational PeLEDs to optimize the performance.

4. Strategies to suppress non-radiative recombination in emitter layer

Over the past few years, the electroluminescent performance (*i.e.*, EQE and luminance) of PeLEDs has seen significant enhancement, which is due in large part to the advances in achieving high-quality perovskite emitter layer. The perovskite emitter layer is usually prepared either in the form of polycrystalline thin film or in the form of nanocrystal thin film. In this section, we provide a critical overview on the strategies employed to suppress non-radiative recombination in perovskite emitter layer, including the manipulation of exciton binding energy, the control of phase distribution and energy transfer, defect passivation, and colloidal nanocrystal synthesis and post-treatment.

4.1 Strategies for reducing non-radiative recombination in perovskite polycrystalline thin film

Unlike the active layer in PSCs, where the perovskite film is flat and uniform with large grain size to achieve efficient exciton diffusion and dissociation, the perovskite grain size in PeLEDs needs to be decreased, as the smaller crystals are desirable to spatially limit the diffusion length of excitons or charge carriers and reduce the possibility of exciton dissociation into carriers for maximizing radiative recombination.[8] As a result, the use of PSCs' deposition procedures in making PeLEDs could not meet the demands for making highly efficient PeLEDs. In this section, we provide a critical overview on the strategies employed to suppress non-radiative recombination in perovskite emitter layer based on polycrystalline films related to the manipulation of exciton binding energy, the control of phase distribution and energy transfer, defect passivation, and perovskite nanocrystal including colloidal nanocrystal synthesis and post-treatment.

4.1.1 Manipulation of exciton binding energy (E_b). Larger E_b promotes faster radiative recombination and further boosts the electroluminescence efficient. Unfortunately, three-dimensional (3D) perovskite with large grain size displays a small E_b (tens meV), leading to slow free electron–hole radiative recombination and limiting the performance of PeLEDs.[65,90,91] Therefore, reducing exciton diffusion length (L_D) and spatially confining charge carriers are required in a 3D polycrystalline film to promote radiative recombination. An effective way to get short L_D is decreasing the grain size of 3D perovskite film (Fig. 3(a and b)). Thus, several strategies have been developed to reduce the crystal size in polycrystalline films, including small molecular assisted film growth,[21–24] anti-solvent modification,[49] anti-solvent vapor treatment,[92] interface layer modification,[30] which enhance the EQE from less than 1% to over 20%.

Converting 3D into quasi-2D perovskite below the Bohr diameter can increase E_b.[25,26] Moreover, the quasi-2D perovskites are rising as potential luminescent materials since the cascade energy landscape empower efficient exciton transfer from wide band to narrow band, which then leads to radiative recombination. Recently, Snaith's group[53] (Fig. 3(c)) discovered that the incorporation of butylammonium (BA) into the 3D lead

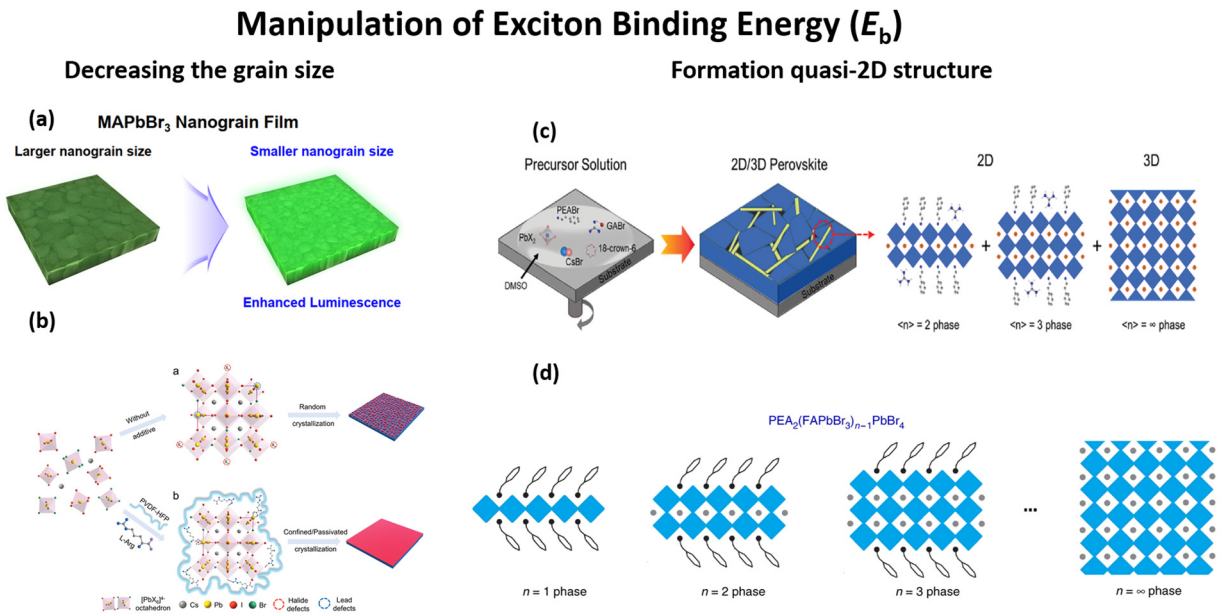

Fig. 3 (a) Schematic illustrations decrease the grain size of $MAPbBr_3$ to enhance luminescent properties. Reproduced with permission from ref. 8. Copyright © 2015, American Association for the Advancement of Science; (b) Schematic illustration of the crystal growth and surface passivation of $CsPbI_{3-x}Br_x$ polycrystalline thin films regulated by poly(vinylidenefluoride-*co*-hexafluoropropylene) and L-arginine. Reproduced with permission from ref. 23. Copyright © 2020 Wiley-VCH GmbH; (c) processing and structural illustration of the 2D/3D perovskite films. The films were prepared by one-step spin-coating a precursor solution containing guanidine hydrobromide (GABr) as an inducer to subsidiary generate oriented 2D perovskite phase. Right is the crystal structure, where GABr as the "spacer" occupies interlayer position similar to PEABr. Reproduced with permission from ref. 66, Copyright © 2020 Wiley-VCH Verlag GmbH & Co. KGaA, Weinheim; (d) scheme of $PEA_2(FAPbBr_3)_{n-1}PbBr_4$ phases, which means that the addition of insert-layer molecules can form quasi-2D perovskite phases. Reproduced with permission from ref. 25. Copyright © 2018, The author(s), Springer Nature.

halide perovskite can form quasi-2D and 3D grains, accompanied by the enhancement of PL intensity. Fig. 3(d) shows another example of the formation of quasi-2D perovskites by introducing phenylethylammonium bromide (PEABr) in the precursor, which results in an increased PLQY of 57.3%.[25]

Despite small grain size can spatially confine the excitons for radiative recombination, the amplified carrier density can also lead to enhanced Auger recombination.[20] In addition, high E_b would speed up the Auger process due to the enhanced Coulomb electron–hole interaction.[20,93] Such interaction can cause an uneven distribution of carriers in space, thus increases the probability of energy transfer to a third carrier and accelerates the Auger process.[94] Therefore, E_b should be judiciously controlled in order to maximize radiative recombination while suppress the Auger recombination loss.[95] For example, in quasi-2D perovskites of $PEA_2(FA_{0.7}Cs_{0.3})_{n-1}Pb_nBr_{3n+1}$ (n = 2, 3,...,∞), Yuan's group found that the low n value perovskite with high E_b cannot reserve the high PLQY and achieve a high brightness under high current density due to the Auger recombination, while high n value with lower E_b perovskite exhibits lower PLQY roll-off because of reduced Auger recombination rate. As a result, the devices-based n = 3 achieved the highest EQE under low current density. The EQE of LEDs declined with the increase of n values (n > 3), and the n = 10 device showed a peak luminance of 91 650 cd m^{-2}.[95] As the Auger recombination rate is proportional to the materials' exciton binding energy, another work in the same group have found that introducing high-polar organic cation, *p*-fluorophenethylammonium (*p*-$FPEA^+$), into the "A-site" of the quasi-2D perovskites resulted in a reduced E_b. To compensate for PLQY decline induced by the decreased first-order exciton recombination rate, authors have explored a molecular passivation agent, CF_3KO_3S, to reduce trap-assisted recombination rate. The modified devices exhibited a peak EQE of 20.36% with a record luminance of 82 480 cd m^{-2} thanks to the suppressed Auger recombination at high current density.[20]

4.1.2 Uniform phase distribution. The quasi-2D perovskite usually contains a mixed phase (different n value), and phase impurity could lead to low emission efficiency.[25] In addition, low quasi-2D phase (n = 1) tends to show severe non-radiative recombination due to strong exciton–phonon coupling.[78,96] Thus, if the films reduce the dispersity in lower n phases and increases the proportion of larger n phases (or a certain n phase), the PL intensity would enhance. Sparked by this idea, inorganic salt, NaBr, was added into the quasi-2D perovskites to suppress the formation of low phases in the perovskite layer (Fig. 4(a)), which improve the PLQY of the sky-blue emitting perovskite films from 39 to 67%.[97] Furthermore, an intriguing method[89] has been proposed by Zhong's group that the use of dual-ligand inhibited the formation of small n and large n domains and thus narrows down the quantum well width with central domination of n = 4, which can assemble the carrier at certain n phase and increase the PLQY.

Meanwhile, the addition of interlayer ligand in quasi-2D perovskite should be rationally chosen, preventing the formation of isolated domains of organic phase and perovskite phase.

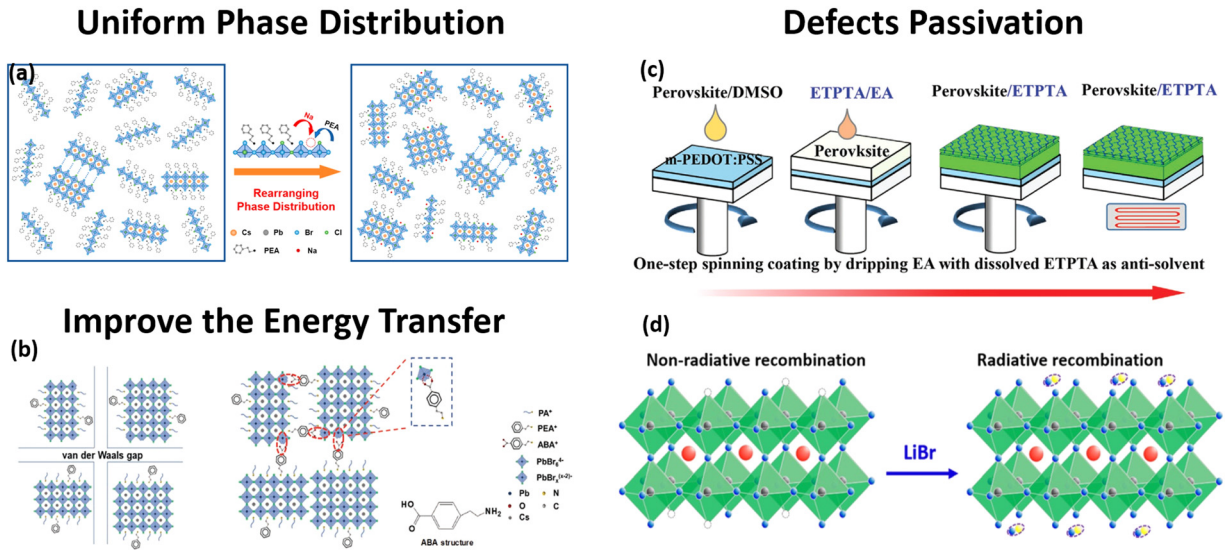

Fig. 4 (a) Schematic illustrated the rearrangement of phase distribution by adding Na^+ in quasi-2D perovskites. Reproduced with permission from ref. 97, Copyright © 2020 American Chemical Society; (b) schematic illustration of the addition 4-(2-aminoethyl)benzoic acid (ABA) into perovskite can enhance the interaction between neighbouring perovskite layers. Reproduced with permission from ref. 101, Copyright © 2020 Wiley-VCH GmbH; (c) schematic illustration of the preparation process of adding ethoxylated trimethylolpropane triacrylate (ETPTA) into antisolvent to passivate the defects. Reproduced with permission from ref. 7, Copyright © 2021 Wiley-VCH GmbH; (d) schematic depicting the surface halide vacancies of $CsPbBr_3$ perovskite films and passivated by organic molecules of PEABr and inorganic molecules of LiBr. Reproduced with permission from ref. 27. Copyright © 2019 Wiley-VCH Verlag GmbH & Co. KGaA, Weinheim.

Such phase separation would weaken the dielectric confinement effects. The dielectric confinement arises from the different dielectric constants between the perovskite phase and organic components, which also contribute to the enhancement of PLQY.[21,98] The low dielectric constant of the adjacent organic layers provides poor shielding of the electrons and holes in the inorganic layers.[99] If the amount of interlayer molecules of quasi-2D perovskite or the organic modified additives is higher than the threshold values, the organic phase may form, which could weaken the dielectric confinement effect. Taking the case of adding of PEABr into the $CsPbBr_3$ as an example, small ratio (40%) of PEABr impedes perovskite crystal growth and leads to smaller crystallites, while the higher PEABr concentrations promote the formation of PEABr organic phase, which weakens the dielectric confinement effects and serves as a non-radiative recombination channel.[21]

The introduction of certain small molecule additives can not only promote the uniform phase distribution, but also play an important role in defects passivation. A recent work from Sargent's group showed that the incorporation of fluorinated triphenylphosphine oxide additive (TFPPO) plays a bifunctional role in a reduced-dimensional perovskites (RDP). The fluorine atoms in TFPPO could form a hydrogen bond with large cation PEA, limiting their diffusion during RDP film deposition and consequently resulting in a monodispersed quantum well. Besides, phosphine oxide (P═O) could also heal the traps by coordinating with unsaturated Pb^{2+} sites. These RDP thin films with narrowband emission and high PLQY achieved a champion EQE of 25.6%.[100] Further comprehensive discussion about the defect passivation by introducing molecular additives will be provided in Section 4.1.4.

4.1.3 Improve the energy transfer among different phases. The inadequate energy transfer from wide to narrow-band phase in mixed phases quasi-2D perovskite leads to multiple emission peaks and low PLQY, which is a undesired phenomenon in PeLEDs and should be eliminated to improve the performance.[97,101] The typical interlayer organic cations can only bind to inorganic perovskite layers at one side and hence leave a van der Waals gap between adjacent cations.[102] The van der Waals gap among quasi-2D perovskite layers will induce a loose space, causing poor radiative recombination rate in the perovskite. Consequently, a bifunctional ligand with amino and carboxylic is strategically introduced into the perovskite to diminish the weak van der Waals gap between individual perovskite layers for promoting coupled quasi-2D perovskite layers. As a result, the PLQY increases from 45.5% to 63.5% (Fig. 4(b)).[101]

Similarly, modulating the transport property of carriers in quasi-2D/3D hybrids structure could boost the recombination efficiency of electrons and holes, which in return enhances the radiative recombination. In other words, creating a facile cascade channel to induce energy transfer from the wide into narrow bandgap in combined quasi-2D and 3D hybrid structures can inhibit free charge diffusion and thus increase the proportion of radiative recombination.[66] Equally importantly, creating stable and efficient heterostructures between quasi-2D and 3D domains can consequently inhibit undesired trap-assisted recombination and further boost the PL intensity.[53]

4.1.4 Defects passivation. Defect passivation has been proven as an effective way to reduce deep level trap-assisted non-radiative recombination losses in PSCs.[61,103] Lessons learned from PSCs should be applicable to PeLEDs as well. However, it

is noted that the grain size of perovskite polycrystalline films in PeLEDs are normally much smaller than that in PSCs, which results in a much higher defects concentration. These defects would act as non-radiative recombination centres and thus decrease the emission efficiency. In addition, in order to enhance the opportunity of electron–hole radiative recombination in the emitter layer, the thickness of perovskite layers in PeLEDs is almost ten times thinner than that in PSCs. Such a thin film would readily result in poor morphology and low film quality, with pinholes potentially serving as non-radiative recombination centres. Therefore, it is necessary to seek some effective methods for passivating defects.

Additive engineering is one of the most effective approaches to passivate the undesirable defects and suppress the non-radiative recombination within perovskite polycrystalline film. For convenience, most additives are directly dissolved in the precursor of perovskite,[22,27,104] which can mitigating both shallow and deep defects in the bulk, at the surface, or on the grain boundaries.[10] In addition, in order to reduce the interfacial defects, the additives can be introduced into anti-solvent and deposited on the perovskite layers (Fig. 4(c)).[7] Also, during the antisolvent process, small organic molecules could penetrate into the perovskite film along the grain boundaries to restrain pinholes, further reducing non-radiative recombination.[7] Abundant additives have been utilized to passivate the defects and successfully suppressed the non-radiative recombination centres. For example, the introduction of bifunctional group including amino and carboxylic molecular can remove metallic Pb defect, which is a major non-radiative recombination center.[101] By suppressing such trap state, the PLQY was increased from 45.5% to 63.5% and a high-performance PeLEDs with EQE of 10.11% was achieved. The adding of LiBr can create a Br-rich environment to prevent the aggregation of free Cs^+ ions on the grain surface, and thus passivate Br vacancies to reduce non-radiative recombination centres (Fig. 4(d)).[27] As a result, a peak EQE of 16.2%, as well as a high maximum brightness of 50 270 cd m^{-2}, are achieved. The sulfonic group of zwitterion 3-aminopropanesulfonic acid (APS) can simultaneously passivate deep and shallow level defects in perovskites *via* coordinate and hydrogen bonding, which improve the EQE from 9% to 19.2%.[105] In summary, these additives can be classified as organic and inorganic, which can passivate shallow defects and even deep level defects.[4,20]

Apart from the prevalent method of additive engineering, other methods are also developed to remove defects, which include vapor-assisted crystallization technique,[106,107] doping metal ions (Rb),[107] cross linked strategy,[28] and so forth.

4.2 Strategies for reducing non-radiative recombination in perovskite nanocrystals thin film

Both colloidal synthesis and post-treatment are critical for obtaining high-quality perovskite nanocrystals with near-unity PLQY. In particular, the surface chemistry engineering including ligand exchange and surface passivation merits more attention to realize simultaneous improvement of both optical and electrical properties of perovskite nanocrystals.

4.2.1 Advanced synthesis methods. In order to minimize the non-radiative recombination, perovskite nanocrystals are expected to be defect-free and have near-unity PLQY. Several synthetic protocols have been developed for the synthesis of perovskite nanocrystals,[69,70,108] among which the hot injection method is the most widely used because the resulting perovskite nanocrystals usually have narrow size distribution and high PLQY. Here, we summarize the key points that warrant attention when performing hot injection synthesis to obtain high quality nanocrystals.

In typical perovskite nanocrystals synthesis, lead halides always serve as both cation and anion precursor. The molar ratio of Pb-to-Cs is typically set as $\sim$3.76 for getting pure crystal phase distribution with good morphology.[109] Although this "two-precursor" method can produce perovskite nanocrystals with PLQY among 60–90%,[110] it still hinders the possibility of studying the desired ion stoichiometry to get high PLQY. In order to overcome such restrictions, the "three-precursor" hot injection approach has been developed (Fig. 5(a)),[112] in which the source of lead and halide respectively come from PbO and small halide molecular, including ammonium salts,[111,112] *n*-bromosuccinimide halide,[113] benzoyl halides,[114] and phenacyl halide.[115] Such method can provide halide-rich environment during the synthesis, which can effectively remove the non-radiative recombination process at halide-vacancies defects. Therefore, control the ratio between different precursor randomly is essential to get high luminescent nanocrystals.

The as-synthesized nanocrystals were either halide-deficient or uncoordinated Pb(II) in the lattice and on the surface, which are the main recombination centres of non-radiative.[116] The utilization of extra metal halide has been offered as a popular way for removing these flaws.[117–120] With excess $ZnBr_2$, the PLQY of $CsPbBr_3$ from blue to green emitting are among 80 to 95%.[117] Also, $CuCl_2$ can also help the Mn-doped $CsPbI_3$ nanocrystals to improve the PLQY.[119] In both cases, the defects are repaired by adding excess halides without incorporation of Zn^{2+} or Cu^{2+} into the lattice. In some cases (Fig. 5(b)), the adding of metal halide can incorporate into perovskite to increase short-range order of the lattice, and simultaneously eliminate the halide vacancies by increasing formation energy of defects to boost the luminescence.[118,121] Some trivalent ion (such as Er^{3+} and Fe^{3+}) can even suppress intrinsic deep traps in $CsPbCl_3$ to increase PLQY.[122,123] Intriguingly, Auger recombination can be suppressed by introducing different types of metal halide into nanocrystals, such as chloride into iodide.[124] Besides metal halide, different kind of chemical species that can strong adhere to the nanocrystals are adapted to improve the luminescent efficiency, including alkylphosphine,[125] quaternary alkylammonium,[126] crosslinking component.[127]

Nanocrystals with approximately unity high PLQY are generally manufactured at high temperatures.[119,128] However, a phase transition may be noticed very instantaneously, which cannot be terminated even with ice bath cooling.[129] Take cubic $CsPbCl_3$ and orthorhombic $CsPbBr_3$ as examples, they would transfer to corresponding non-emitting tetragonal phases during annealing (>180 °C).[129,130] Therefore, alkylammonium halides

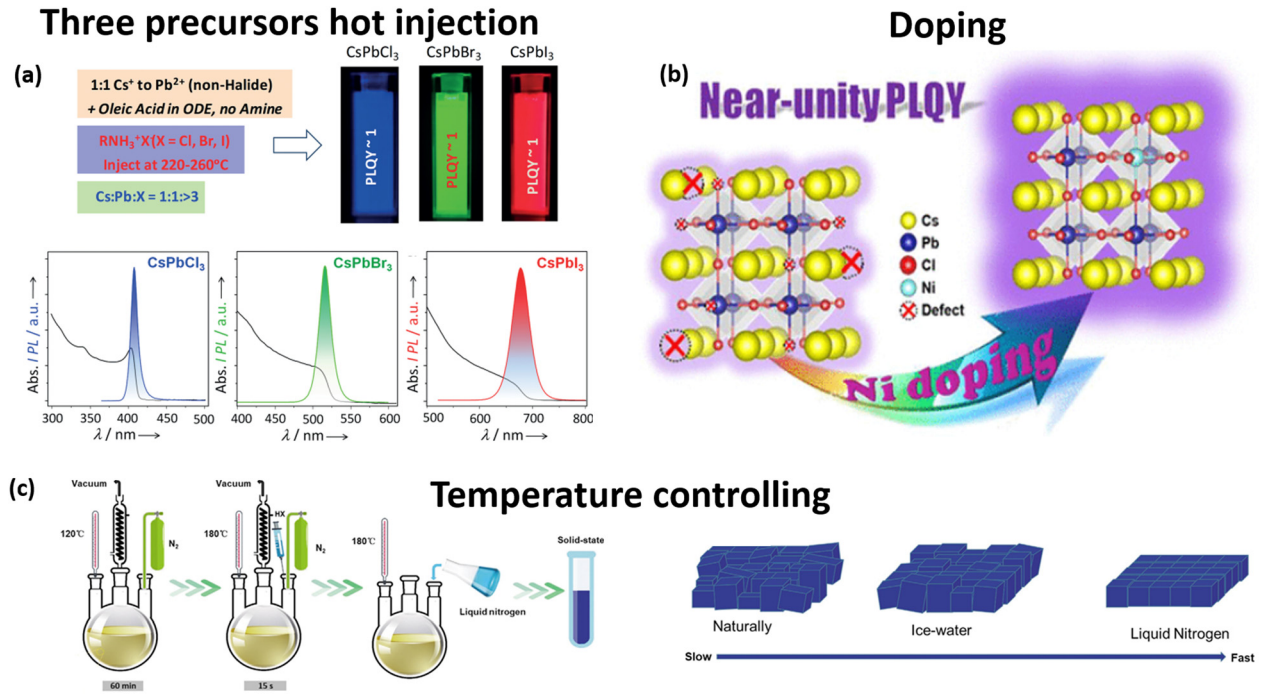

Fig. 5 (a) Schematic representation of the reaction giving near unity quantum yields in $CsPbX_3$ nanocrystals. Digital photographs of $CsPbCl_3$ (blue), $CsPbBr_3$ (green), and $CsPbI_3$ (red) nanocrystals dispersed solution under irradiation (365 nm). Absorption (black line) and corresponding PL spectra (coloured) of $CsPbCl_3$, $CsPbBr_3$, and $CsPbI_3$ nanocrystals obtained in our approach showing near unity quantum yields. Excitation wavelength was 350 nm. Reproduced with permission from ref. 112. Copyright © 2019 Wiley-VCH Verlag GmbH & Co. KGaA, Weinheim; (b) diagram showing Ni doping in $CsPbCl_3$ nanocrystals can boost the PLQY to near unity. Reproduced with permission from ref. 118. Copyright © 2018 American Chemical Society; (c) the schematic diagram of the synthesis method with liquid nitrogen cooling and the relationship between cooling rate and crystal quality. Reproduced with permission from ref. 131. Copyright © 2020 WILEY-VCH Verlag GmbH & Co. KGaA, Weinheim.

are used to restrict these phase changes and the obtained nanocrystals can endure the annealing for hours.[127] Furthermore, after injecting Cs or another precursor, the nucleation and growth processes might occur simultaneously in a matter of seconds (less than 10 s), requiring rapid cooling to maintain the light-emitting phase of the nanocrystals.[116,131] Recent research reveals that ultrafast cooling rate (50 K s^{-1}) by liquid nitrogen can effectively lower the reaction thermodynamic energy of the system below the threshold (Fig. 5(c)). Thus, it can rapidly hinder the further growth of nanocrystals and avoids the additional nucleation, achieving uniformity grain size and better crystallinity.[131] The $CsPbBr_xCl_{3-x}$ nanocrystals synthesized through such method have been achieved the PLQY of 98%.[131]

4.2.2 Post-treatment. The surfactants with long carbon chains can easily tune the nanocrystals' size and shape during the synthesis process, and anchor on the surface of nanocrystal to reduce the probability of non-radiative recombination.[132] However, once the colloidal nanocrystals are transferred to film to fabricate the optoelectronic devices, this long chain ligands will impede the carrier transfer and reduce the coupling among the nanocrystals.[1] Furthermore, they can produce oily film with poor morphology, causing non-radiative losses due to the formation of non-radiative recombination centers.[133] Thus, it is necessary to exchange the long insulting ligands with small conductive ligands to get an efficient carrier injection and radiative recombination properties.

Purified the nanocrystal with poor solvent (such as methyl acetate, ethyl acetate, pentanol, or ever acetone) has been identified as a practical method to remove the insulting ligands.[134] However, the excessive detachment of ligands leads to insufficient passivation of the surface defects, resulting in poor stability and facilitating non-radiative recombination. What is worse, recent research indicated that the left uncoordinated halide ions on the surface can even evolve into deep defects.[135] And the reduced barrier among the nanocrystals promotes the aggregation and regrowth of perovskite.[136] Therefore, additional ligands or additives can be introduced in this process or after the first cycle of purification to passivate the defects and further prevent non-radiative recombination.[137]

The ligands can be classified as L, X, and Z types by the number of electrons (2, 1, and 0, respectively) that the ligand donates to the surface atoms (Fig. 6(a)).[138] L-type ligands usually share a lone electron pair with Pb and act as Lewis bases; while Z-type ligands accept a lone electron pair from the halide anions acting as the Lewis acids. Common X-type ligands with one function group can either passivate the halide anion or Pb site. The zwitterionic/bidentate ligands in X type with two functional groups in positive and negative charges can simultaneously bind to two sites. Due to the ionic nature, the ligands used for capping nanocrystals and maintaining/improving the bright luminescent are fall into the X- and L-type categories.[137]

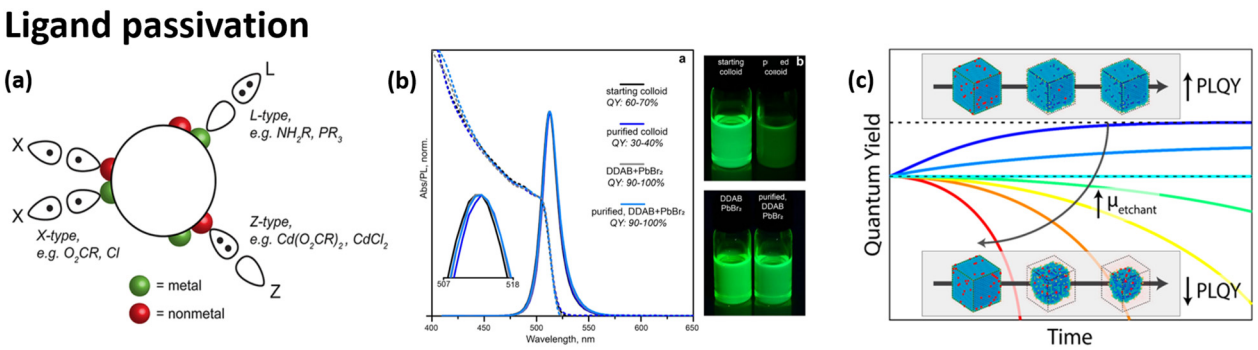

Fig. 6 (a) Nanocrystal ligand binding motifs according to the covalent bond classification method. Reproduced with permission from ref. 138. Copyright © 2018 American Chemical Society; (b) comparison of the steady-state absorption and PL spectra for the starting colloid and the same colloid subjected to several treatments, which suggests the synergistic passivation of DDAB and $PbBr_2$ can improve and keep the PLQY. Reproduced with permission from ref. 139. Copyright © 2018 American Chemical Society; (c) relationship between PLQY and different chemical potentials of thiocyanate etchant. Reproduced with permission from ref. 146. Copyright © 2019 American Chemical Society.

Halide vacancies is one of main defects in causing non-radiative recombination, which can be effectively passivated by organic halogens in X-type. The excess halide-rich environment can produce a halide-rich surface layer, which can form a quantum-well-like band alignment since the bandgap of surface is larger than the core nanocrystals, guaranteeing the excitons generation and high-rate radiative recombination.[70] The A site vacancies is another non-radiative recombination centres, which normally can be refilled with the ammonium cation and zwitterionic ligands. As these two defects appear simultaneously during the purification process, there is a need in combining the properties of different ligands to get high PLQY. The coexisting of didodecyl dimethyl ammonium bromide (DDAB) and lead bromide in post treatment process can endow $CsPbBr_3$ nanocrystals with high PLQY of 95–98%, even retaining after three to four cycles of washing (Fig. 6(b)).[139] In some cases, the defects can induce Auger recombinations[140] and treated with ligands can remove the defects and suppress Auger processes effectively.[141]

Due to intrinsically ionic and highly dynamic nature of perovskite, the ligands are in a highly dynamic equilibrium between free and bound state.[142] Ligands can easily detach from the surface and left unbonded lead or halide ions on the surface, causing more vacancies. Even in the fresh sample, the weak affinity of the ligand can lead coalescence of the nanocrystals, and become worse with aging.[143] The binding affinity between the ligands and the surface atoms should be strengthened. According to a recent study, defects caused in purification process can be avoided by increasing the coordination ability between the Pb^{2+} and the thiol group of ligands, resulting in nanocrystals with a PLQY of 98%.[144] In high affinity system, the post treatment with octyl-ammonium sulfate can produce a $CsPbX_3/PbSO_4$ core/shell heterostructure, which can improve the radiative recombination and exhibit excellent optical properties.[145]

Etching the surface selectively represents a promising pathway for mitigating the optical defects in perovskite nanocrystals.[146,147] By adjusting concentration or strength of the chemical etchant to change the etchant chemical potential, we can systematically study the etching extent varying from only a few lead atoms to nearly all the lead atoms of the nanocrystal (Fig. 6(c)). It is difficult to completely eliminate non-radiative recombination defects to produce near-unity PLQY if the chemical potential is too low. When the chemical potential is too high, the etching reaction becomes nonselective. Only by choosing an appropriate concentration of an etchant with an appropriate lead binding strength can we selectively remove the non-radiative recombination traps on the surface of nanocrystals, and then improve the PLQY reliably.[146]

5. Device engineering

As discussed earlier, the defects located at various interfaces as well as the non-optimal energy level alignment within the device are also considerable pathways of non-radiative recombination. Therefore, in addition to the advances in achieving highly luminescent perovskites, device engineering also plays a pivotal role in minimizing the non-radiative recombination loss in PeLEDs. In this section, we present the most recent developments in architectural design and interfacial modification with the goal of increasing PeLEDs' radiative recombination.

5.1 Energy level alignment

The unbalanced carrier injection within PeLEDs can cause carriers accumulation at the interface, which gives rise to non-radiative recombination and significant luminescence quenching.[148,149] To address such issue, it is highly desirable to improve the energy level alignment among different layers as well as to balance the carrier mobility between the ETL and HTL, which have proven effective in achieving balanced carrier injection within PeLEDs.[33]

The mismatch of energy level between perovskite layer and CTLs could cause the accumulation of charge carriers at the interfaces, which reduces the possibility of radiative recombination within the emitter layer while increases Auger recombination at the interfaces. To optimize the injection of charges into the perovskite layer, the energy barrier for CTLs/emitting

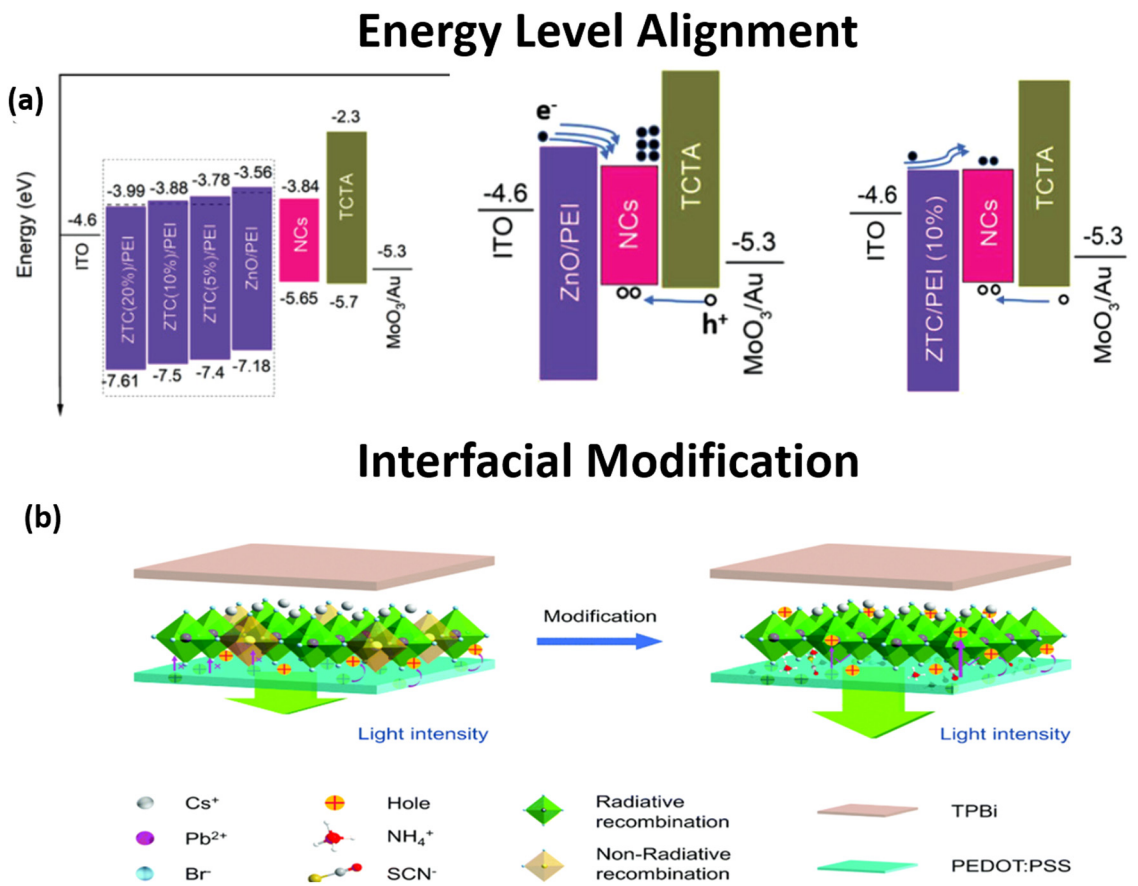

Fig. 7 (a) Device energy-level diagram for MXene modified transfer layer in the PeLEDs (left) and charge carrier injection and recombination mechanisms for 0% (middle), and 10% (right) MXenes based devices. ZTC in the diagram represents ZnO–Ti_3C_2. Reproduced with permission from ref. 150. Copyright © 2020 The Authors. Published by Wiley-VCH GmbH; (b) schematic illustration of the interface defect passivation mechanism of perovskite films *via* ammonium thiocyanate modification. Reproduced with permission from ref. 155. Copyright © 2021, The Royal Society of Chemistry.

layer should be minimized. In addition, the desired CTLs also should possess electron/hole-blocking abilities for HTLs and ETLs, respectively. Limited by the energy levels of commonly employed CTLs, the modification of transfer layers to align perovskite emitter is a prevalent method in PeLEDs.[150] As shown in Fig. 7(a), the addition of MXenes can modified the working function of transfer layer and creates more balanced charge carrier transfer in PeLEDs.[150] In the typical device structures of ITO/poly(3,4-ethylenedioythiphene):polystyrene sulfonate (PEDOT:PSS)/perovskite/2,2′,2″-(1,3,5-benzinetriyl)-tris-(1-phenyl-1-*H*-benzimidazole) (TPBi)/LiF/Al, the efficiency is limited by a lower work-function of the widely used PEDOT:PSS (4.9 eV) compared to perovskite emitting material. In order to tackle this problem, poly(styrene sulfonate) sodium salt (PSS-Na) was incorporated in the PEDOT:PSS solution to increase the work function of HTLs and better aligned with conduction band of perovskite. Besides, the upper insulting polymer increase the carrier quenching blocking ability in the interface of HTL/perovskite, leading to a longer lifetime of perovskite film on modified PEDOT:PSS than that on pristine one. Accompanied with the passivating treatment, the green and blue LEDs showed a champion EQE of 22.5% for green perovskite LEDs and 12.1% for blue LEDs, respectively.[7,104]

The capability for conveying charges varying in light of p/n-type semiconductors. Normally, electrons in ETL transfer much faster than that of the holes in HTL, causing non-uniform distributions of electron and hole in the emitter layer both in spatial and time scale.[15] This would result in a higher ratio of Auger recombination accompany with a smaller radiative recombination rate, especially at the interface of emitter layer/CTLs.[151] When holes and electrons have a significant transfer rating mismatch, they can recombine within the transfer layers, lowering the possibility of radiative recombination in the emitter layer. In order to tackle this issue, many factors should be taken into consideration for designing the devices, including the thickness of the transfer layer,[152] improving/decreasing the transfer ability.[150] In the architecture of ITO/PEDOT:PSS/poly[bis(4-phenyl)(2,4,6-trimethylphenyl)amine] (PTAA)/perovskite/TPBi/LiF/Al, more holes are injected into nanocrystals and overflow into the ETL of TPBi due to different carrier mobility between PTAA and TPBi, resulting in Auger recombination and interface non-radiative recombination. The introduction of the bilayered electron transport layers including a low mobility ETL (TPBi) and a high mobility ETL (2,4,6-tris[3-(diphenylphosphinyl)phenyl]-1,3,5-triazine) (PO-T2T) provides a feasible route to offset the ability difference in charge mobility,

leading to a champion EQE of 21.63% coupled with a significant improved device stability.[16]

5.2 Interfacial modification

Due to interfacial tension, the solution of perovskite precursors or nanocrystals cannot entirely spread out on the transfer layer in some cases. As a result, the emitter layer would be in poor morphology, in which the pinhole would appear in the thin film, or even discontinuous film with island or branch-like crystals. Perovskites may only be deposited on a restricted range of transporting materials as a result of this, which may limit their potential for producing brighter PeLEDs. The mainstream HTL are limited within several materials, including PEDOT:PSS, PTAA, poly(*N*,*N*′-bis-4-butyl phenyl-*N*,*N*′-bisphenyl)-benzidine (poly-TPD), poly(9-vinylcarbazole) (PVK), and nickel oxide (NiO_x). To tackle this issue, interface modification is used at the top or bottom of emitter layer. Through modification, not only can we adjust the injection capacity of holes and charges into the emission layer to balance the charge carrier density, but also passivate the defects that generate non-radiative recombination. In addition, it is worthy noted that the experience and methods could be different in solving the interface problems for polycrystalline film based and the nanocrystals based PeLEDs. Because these two kinds of precursors are normally dissolved in polar and nonpolar solvent, respectively, which can influence of the wettability between the transfer layer and the emitter layer.

Modifying the carrier transfer layers can influence the interface, especially the one adjusted to the emitter layer. Here we use the most popular HTL, PEDOT:PSS, as example to illustrate such effects. Owing to distinguished hole mobility (1.23×10^{-2} cm^2 V^{-1} S^{-1}) and transparency property, PEDOT:PSS has been widely used in PeLEDs.[7,55,101] Nevertheless, the morphologies and crystal quality of perovskite films spin-coated on convention PEDOT:PSS layer is uncontrollable, resulting in interface-induced non-radiative defect.[153,154] To solve this issue, additives were added into PEDOT:PSS to manipulate crystallinities, morphology, energy level, and carrier transfer properties. For example (Fig. 7(b)), the adding of organic additive ammonium thiocyanate into PEDOT:PSS can decrease the contact angle, indicating the improved hydrophilicity and wetting properties of the precursor solution dropped on the modified PEDOT:PSS substrate. Moreover, through the scanning electron microscopy, polycrystalline perovskite with clusters transformed into uniform and dense cubic perovskite crystals. As a result, the modified PEDOT:PSS significantly improved light intensity and EQE achieved 460% enhancement.[155] Moreover, conducting polymer,[7,156] small organic molecules,[157] inorganic salt[158] are also used in modifying the PEDOT:PSS to remove non-radiative recombination centres in interface between hole injecting layers and perovskite layers, and further improve the PL intensity dramatically. Similarly, the methods used to the most common HTL can also be used to other transfer layers.

Apart from the modification of carrier transfer layers, the modification can also be applied in the emitter layers itself. The surface passivating species, such as alkali metal halide additives, not only can influence the growth of the polycrystalline, but also can significantly smooth the film with less pinholes and further reduce non-radiative recombination at the surface.[159] Some amino additives can even both bind with the emitter layer and the charge transfer layer at the same time, thus enhanced the exciton recombination.[29]

6. Future perspectives

The non-radiative recombination pathways have been systematically discussed above, along with various characterizations and tactful means of mitigating such losses. Benefiting from a deep understanding of defect passivation in PSCs, the performance of PeLEDs has seen a rapid rise in the past few years. However, we are still at the early stages of understanding and addressing the losses associated with non-radiative recombination in PeLEDs. Substantial efforts need to be devoted to developing defect-free PeLEDs with minimized non-radiative recombination losses and purse outstanding prolonged device lifetime towards practical application. The future perspectives are outlined in Fig. 8 with details discussed below.

6.1 Advanced characterizations

The charge carrier recombination process is extremely complex in PeLEDs, with single- and multi-body participation in different situations. It is hard to get a comprehensive understanding of each non-radiative pathway through single characterization. For example, due to difficulties in controlling the degree of charging, studies of Auger decay have mostly focused on charge neutral multiexcitons, such as biexcitons. The charged specie, trion, has been less thoroughly investigated, although it determines the luminescence properties of materials. In addition, many recombination processes occur within few ps. However, the time resolution of typical time-correlated single-photon counting (TCSPC) employed in transient studies is on the order of 100 ps, and numerous ultrafast phenomena have not been thoroughly investigated.[160] In addition, direct monitoring of the non-radiative recombination in the device has rarely been investigated, which is partially due to the complicated processes under device operation. Moreover, other mechanisms (such as carrier leakage in nitride-based LEDs[161]) that could lead to increased Auger recombination rate should be discovered and investigated. Thus, advanced characterization techniques with higher time-resolution (even attosecond) should be developed in order to draw a full picture of non-radiative recombination processes.

6.2 Regulating the crystallization process

Attentions should be paid to control the nucleation and growth of crystals, both for polycrystalline film and colloidal nanocrystals. The distribution inhomogeneity of different n domains in quasi-2D polycrystal film impedes the efficient energy transfer within the emitter layer, leading to spatial and energetic disorder and resulting low performance.[100] Reduced-dimensional perovskite distribution management to obtain a monodispersed

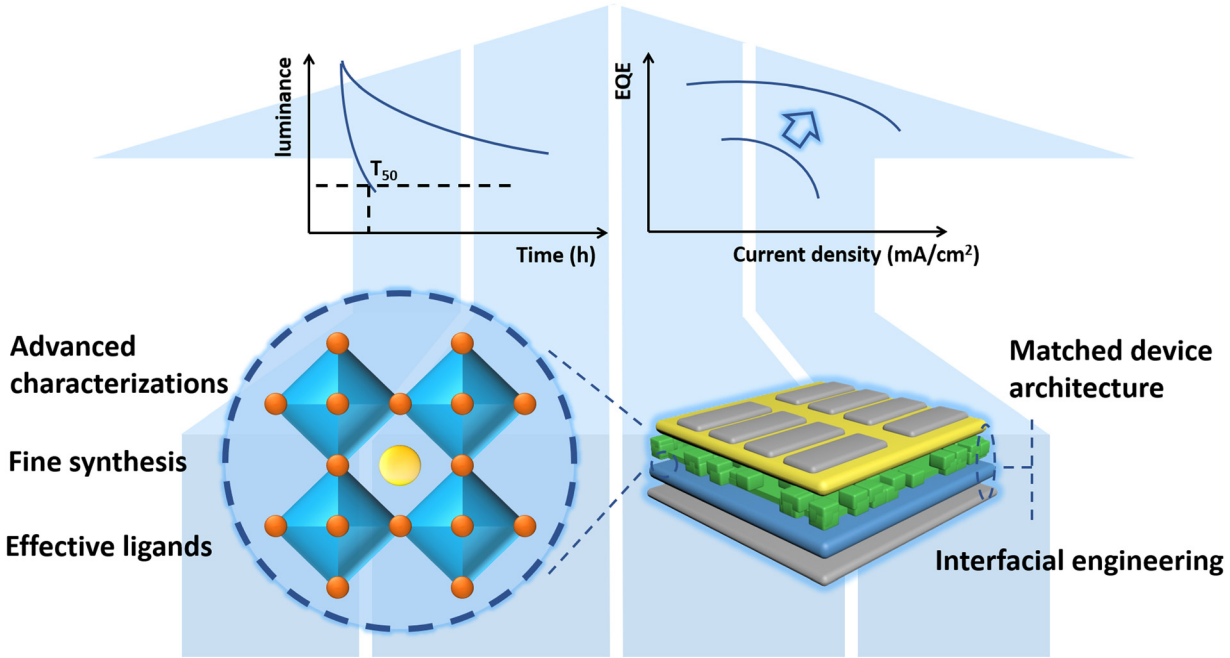

Fig. 8 Future opportunities in minimizing non-radiative recombination towards high-efficiency and long-lifetime PeLEDs.

quantum well (QW) thickness distribution is highly desired for narrow emission and low non-radiative recombination losses. Additive engineering (like NaBr, KBr, *etc.*) could be an effective way to affect the crystal nucleation and growth, as well as reducing the traps in the duration of deposition of perovskite precursor.[97,162] The application of PeLEDs requires a thorough understanding of the critical point in the processes of bi-molecular recombination and Auger recombination, as well as the accomplishment of the highest EQE and brightness before this stage, which compelled us to exploit advanced characterization for analysis of the complicated process.

6.3 Engineering surface ligands for stable perovskite nanocrystals with high PLQY

Emitter layer should possess a good conductivity in devices, especially for the nanocrystals based PeLEDs. Although the ligand exchange approach may enhance the PLQY to near unity and replace low-conductivity ligands with high-conductivity ones, steric hindrance effects and entropic limitations make entirely passivating all defects challenging. To tackle the aforementioned issues in the exchange process, multiple ligands should be considered. Furthermore, without altering or degrading the material, this approach still lacks suitable ligands for successful exchange of long chain ligands. As a result, there is a pressing need to expand the library of usable compounds, particularly those with substantial lead binding strengths. Moreover, although the EQE of perovskite NCs-based LEDs has improved, their lifetime is still lower than that of polycrystalline film LEDs. Designing core/shell structured perovskite nanocrystals based on lessons learned from inorganic quantum dots (*i.e.*, CdSe/ZnS) could be a feasible way to improve the stability of nanocrystals based PeLEDs.

6.4 Suppression of ion migration

The stable perovskite materials play a crucial role in extending the lifetime of PeLEDs, while the improved stability of emitting materials could be modified by incorporation of binary alkali cations, and replacement of MA with FA or Cs.[163] To improve the quality of perovskite layer relate to low trap density, the incorporation of passivation agents (PAs) to achieve the defects free films is not only a prerequisite for achieving a high EQE, but also the non-radiative recombination sites healed by the PAs also could be favourable for maintaining the stable crystal structure of perovskite, and further improving the device durability. The PAs could suppress defects at the grain boundary caused by ions migration or produced during the film preparation process under a high bias. Previous researches have shown that inorganic salts, cross-linking polymers or amino/phosphine oxide/carbonyl-functioned organic molecules treated LEDs have a longer operational time than control ones. Hence, it is still necessary to exploit novel PAs with improved passivation ability, both for the improvement of EQE and stability.

6.5 Interfacial engineering to balance the charge carrier within emitter layer

To retard the severe Auger recombination loss at the interface of perovskite/CTLs, device structure of PeLEDs should be optimized since the comparable charge injection or transportation capability could balance carriers in emitting layer rather than accumulating extra holes or electrons at the interface and result in the non-radiative recombination loss. The introduction of inserting layers not only balances the charge transfer, but it also avoids non-radiative recombination loss and blocks the ions migration through the neighbouring layers. For instance, LiF was employed act as a buffer layer to inhibit of

metal migration and ion migration, enhanced the stability of devices.[164] The principal factors involve in the selection of the insertion layers in the interface of perovskite/CTLs should considering charge balance in perovskite, the interface defects, crystallization of perovskite film, the hydrophilic nature as well as hole/electron blocking ability for ETL/perovskite and HTL/perovskite, respectively.

6.6 Substitution of the direct current driving mode with pulsed current operation

Replacement of current-focusing architecture with pulsed current operation is an effectively mean to minimize the impact of Joule heating and ion migration in operating LEDs.[147,165] Reduced non-radiative recombination pathways and pulsed current operation, in combination with thermal management, show significant potential for prolonging LED lifetime.

The field of PeLEDs is still burgeoning and will continue to flourish in the near future. We envisage that future advances in both understanding and mitigation of non-radiative recombination losses in PeLEDs will soon be translated into further improvement of electroluminescence efficiency and operational stability approaching that of commercial devices, which paves the way for the development of next-generation lighting and display technologies.

Author contributions

H. C. and Y. B. conceived the idea and determined the review structure; H. C., Y. M. wrote the manuscript; Y. B. and Y. S. supervised the manuscript writing and revision. All authors reviewed the manuscript.

Conflicts of interest

There are no conflicts to declare.

Acknowledgements

Y. B. appreciates the funding support from the Australian Research Council through Discovery Early Career Researcher Award Fellowship (DE190101351) and the Discovery Project (DP190102507). Y. B. also acknowledges Shenzhen Institute of Advanced Technology, Chinese Academy of Sciences, for providing a start-up fund. Y. S. acknowledges the financial support from National Science Foundation of China (NSFC 62104234). Y. Z. appreciates the support from National Natural Science Foundation of China (52103279) and Shanghai Sailing Program (21YF1454000).

References

1 J. Park, H. M. Jang, S. Kim, S. H. Jo and T. W. Lee, *Trends Chem.*, 2020, **2**, 837–849.
2 X. K. Liu, W. Xu, S. Bai, Y. Jin, J. Wang, R. H. Friend and F. Gao, *Nat. Mater.*, 2021, **20**, 10–21.
3 Z. K. Tan, R. S. Moghaddam, M. L. Lai, P. Docampo, R. Higler, F. Deschler, M. Price, A. Sadhanala, L. M. Pazos, D. Credgington, F. Hanusch, T. Bein, H. J. Snaith and R. H. Friend, *Nat. Nanotechnol.*, 2014, **9**, 687–692.
4 Z. Liu, W. Qiu, X. Peng, G. Sun, X. Liu, D. Liu, Z. Li, F. He, C. Shen, Q. Gu, F. Ma, H. L. Yip, L. Hou, Z. Qi and S. J. Su, *Adv. Mater.*, 2021, **33**, 2103268.
5 W. H. Jeong, Z. Yu, L. Gregori, J. Yang, S. R. Ha, J. W. Jang, H. Song, J. H. Park, E. D. Jung, M. H. Song, S. H. Park, H. J. Snaith, A. Boretti, F. D. Angelis, D. Meggiolaro, J. Lee, H. Choi and B. R. Lee, *J. Mater. Chem. A*, 2021, **9**, 26750–26757.
6 W. K. Bae, Y. S. Park, J. Lim, D. Lee, L. A. Padilha, H. McDaniel, I. Robel, C. Lee, J. M. Pietryga and V. I. Klimov, *Nat. Commun.*, 2013, **4**, 1–8.
7 Z. Chu, Q. Ye, Y. Zhao, F. Ma, Z. Yin, X. Zhang and J. You, *Adv. Mater.*, 2021, **33**, 2007169.
8 H. Cho, S. H. Jeong, M. H. Park, Y. H. Kim, C. Wolf, C. L. Lee, J. H. Heo, A. Sadhanala, N. Myoung and S. Yoo, *Science*, 2015, **350**, 1222–1225.
9 Q. A. Akkerman, G. Rainò, M. V. Kovalenko and L. Manna, *Nat. Mater.*, 2018, **17**, 394–405.
10 B. Chen, P. N. Rudd, S. Yang, Y. Yuan and J. Huang, *Chem. Soc. Rev.*, 2019, **48**, 3842–3867.
11 J. M. Ball and A. Petrozza, *Nat. Energy*, 2016, **1**, 1–13.
12 W. Zou, R. Li, S. Zhang, Y. Liu, N. Wang, Y. Cao, Y. Miao, M. Xu, Q. Guo, D. Di, L. Zhang, C. Yi, F. Gao, R. H. Friend, J. Wang and W. Huang, *Nat. Commun.*, 2018, **9**, 1–7.
13 J. E. Jeong, J. H. Park, C. H. Jang, M. H. Song and H. Y. Woo, *Adv. Mater.*, 2020, **32**, 2002176.
14 C. M. Wolff, P. Caprioglio, M. Stolterfoht and D. Neher, *Adv. Mater.*, 2019, **31**, 1902762.
15 Z. Yao, C. Bi, A. Liu, M. Zhang and J. Tian, *Nano Energy*, 2022, **95**, 106974.
16 T. Fang, T. Wang, X. Li, Y. Dong, S. Bai and J. Song, *Sci. Bull.*, 2021, **66**, 36–43.
17 A. J. Barker, A. Sadhanala, F. Deschler, M. Gandini, S. P. Senanayak, P. M. Pearce, E. Mosconi, A. J. Pearson, Y. Wu, A. R. Srimath Kandada, T. Leijtens, F. De Angelis, S. E. Dutton, A. Petrozza and R. H. Friend, *ACS Energy Lett.*, 2017, **2**, 1416–1424.
18 M. Xie and J. Tian, *J. Phys. Chem. Lett.*, 2022, **13**, 1962–1971.
19 Y. K. Wang, F. Yuan, Y. Dong, J. Y. Li, A. Johnston, B. Chen, M. I. Saidaminov, C. Zhou, X. Zheng and Y. Hou, *Angew. Chem., Int. Ed.*, 2021, **60**, 16164–16170.
20 Y. Jiang, M. Cui, S. Li, C. Sun, Y. Huang, J. Wei, L. Zhang, M. Lv, C. Qin, Y. Liu and M. Yuan, *Nat. Commun.*, 2021, **12**, 1–10.
21 M. Ban, Y. Zou, J. P. Rivett, Y. Yang, T. H. Thomas, Y. Tan, T. Song, X. Gao, D. Credgington and F. Deschler, *Nat. Commun.*, 2018, **9**, 1–10.
22 Y. Cao, N. Wang, H. Tian, J. Guo, Y. Wei, H. Chen, Y. Miao, W. Zou, K. Pan, Y. He, H. Cao, Y. Ke, M. Xu, Y. Wang, M. Yang, K. Du, Z. Fu, D. Kong, D. Dai, Y. Jin, G. Li, H. Li, Q. Peng, J. Wang and W. Huang, *Nature*, 2018, **562**, 249–253.

23 K. H. Wang, L. Wang, Y. Y. Liu, Y. H. Song, Y. C. Yin, J. S. Yao, J. N. Yang, J. J. Wang, L. Z. Feng and Q. Zhang, *Adv. Opt. Mater.*, 2021, **9**, 2001684.
24 H. Wang, X. Zhang, Q. Wu, F. Cao, D. Yang, Y. Shang, Z. Ning, W. Zhang, W. Zheng, Y. Yan, S. V. Kershaw, L. Zhang, A. L. Rogach and X. Yang, *Nat. Commun.*, 2019, **10**, 1–10.
25 X. Yang, X. Zhang, J. Deng, Z. Chu, Q. Jiang, J. Meng, P. Wang, L. Zhang, Z. Yin and J. You, *Nat. Commun.*, 2018, **9**, 1–8.
26 Z. Chen, C. Zhang, X. F. Jiang, M. Liu, R. Xia, T. Shi, D. Chen, Q. Xue, Y. J. Zhao and S. Su, *Adv. Mater.*, 2017, **29**, 1603157.
27 T. Wu, J. Li, Y. Zou, H. Xu, K. Wen, S. Wan, S. Bai, T. Song, J. A. McLeod and S. Duhm, *Angew. Chem., Int. Ed.*, 2020, **59**, 4099–4105.
28 B. Han, S. Yuan, B. Cai, J. Song, W. Liu, F. Zhang, T. Fang, C. Wei and H. Zeng, *Adv. Funct. Mater.*, 2021, **31**, 2011003.
29 L. Tang, J. Qiu, Q. Wei, H. Gu, B. Du, H. Du, W. Hui, Y. Xia, Y. Chen and W. Huang, *ACS Appl. Mater. Interfaces*, 2019, **11**, 29132–29138.
30 L. Zhang, X. Yang, Q. Jiang, P. Wang, Z. Yin, X. Zhang, H. Tan, Y. M. Yang, M. Wei, B. R. Sutherland, E. H. Sargent and J. You, *Nat. Commun.*, 2017, **8**, 1–8.
31 T. Miyasaka, *Perovskite Photovoltaics and Optoelectronics: From Fundamentals to Advanced Applications*, John Wiley & Sons, 2021.
32 V. K. Khanna, *Fundamentals of solid-state lighting: LEDs, OLEDs, and their applications in illumination and displays*, CRC Press, 2014.
33 A. Liu, C. Bi, R. Guo, M. Zhang, X. Qu and J. Tian, *Adv. Opt. Mater.*, 2021, **9**, 2002167.
34 R. Williams, J. Grim, Q. Li, K. Ucer, G. Bizarri and A. Burger, *Excitonic and Photonic Processes in Materials*, Springer, 2015.
35 J. Ye, M. M. Byranvand, C. O. Martínez, R. L. Hoye, M. Saliba and L. Polavarapu, *Angew. Chem., Int. Ed.*, 2021, **133**, 21804–21828.
36 J. Kang and L. W. Wang, *J. Phys. Chem. Lett.*, 2017, **8**, 489–493.
37 P. T. Landsberg, *Basic properties of semiconductors*, Elsevier, 2016.
38 E. Yoon, K. Y. Jang, J. Park and T. W. Lee, *Adv. Mater. Interfaces*, 2021, **8**, 2001712.
39 Y. S. Park, W. K. Bae, J. M. Pietryga and V. I. Klimov, *ACS Nano*, 2014, **8**, 7288–7296.
40 M. Levinshtein, *Handbook series on semiconductor parameters*, World Scientific, 1997.
41 P. Ščajev, S. Miasojedovas, A. Mekys, D. Kuciauskas, K. G. Lynn, S. K. Swain and K. Jarašiūnas, *J. Appl. Phys.*, 2018, **123**, 025704.
42 J. X. Shen, X. Zhang, S. Das, E. Kioupakis and C. G. Van de Walle, *Adv. Energy Mater.*, 2018, **8**, 1801027.
43 V. I. Klimov, *Annu. Rev. Condens. Matter Phys.*, 2014, **5**, 285–316.
44 Y. Yang, M. Yang, Z. Li, R. Crisp, K. Zhu and M. C. Beard, *J. Phys. Chem. Lett.*, 2015, **6**, 4688–4692.
45 M. Li, Y. Zhao, X. Qin, Q. Ma, J. Lu, K. Lin, P. Xu, Y. Li, W. Feng, W. H. Zhang and Z. Wei, *Nano Lett.*, 2022, **22**, 2490–2496.
46 B. Zhao, Y. Lian, L. Cui, G. Divitini, G. Kusch, E. Ruggeri, F. Auras, W. Li, D. Yang, B. Zhu, R. A. Oliver, J. L. MacManus-Driscoll, S. D. Stranks, D. Di and R. H. Friend, *Nat. Electron.*, 2020, **3**, 704–710.
47 S. Lee, D. B. Kim, I. Hamilton, M. Daboczi, Y. S. Nam, B. R. Lee, B. Zhao, C. H. Jang, R. H. Friend and J. S. Kim, *Adv. Sci.*, 2018, **5**, 1801350.
48 L. Meng, E. P. Yao, Z. Hong, H. Chen, P. Sun, Z. Yang, G. Li and Y. Yang, *Adv. Mater.*, 2017, **29**, 1603826.
49 M. H. Park, S. H. Jeong, H. K. Seo, C. Wolf, Y. H. Kim, H. Kim, J. Byun, J. S. Kim, H. Cho and T. W. Lee, *Nano Energy*, 2017, **42**, 157–165.
50 W. K. Bae, S. Brovelli and V. I. Klimov, *MRS Bull.*, 2013, **38**, 721–730.
51 A. Subramanian, Z. Pan, Z. Zhang, I. Ahmad, J. Chen, M. Liu, S. Cheng, Y. Xu, J. Wu, W. Lei, Q. Khan and Y. Zhang, *ACS Appl. Mater. Interfaces*, 2018, **10**, 13236–13243.
52 D. W. de Quilettes, S. M. Vorpahl, S. D. Stranks, H. Nagaoka, G. E. Eperon, M. E. Ziffer, H. J. Snaith and D. S. Ginger, *Science*, 2015, **348**, 683–686.
53 Z. Wang, Q. Lin, F. P. Chmiel, N. Sakai, L. M. Herz and H. J. Snaith, *Nat. Energy*, 2017, **2**, 17135.
54 M. J. Trimpl, A. D. Wright, K. Schutt, L. R. Buizza, Z. Wang, M. B. Johnston, H. J. Snaith, P. Müller-Buschbaum and L. M. Herz, *Adv. Funct. Mater.*, 2020, **30**, 2004312.
55 M. Liu, Q. Wan, H. Wang, F. Carulli, X. Sun, W. Zheng, L. Kong, Q. Zhang, C. Zhang and Q. Zhang, *Nat. Photonics*, 2021, **15**, 379–385.
56 B. T. Diroll, G. Nedelcu, M. V. Kovalenko and R. D. Schaller, *Adv. Funct. Mater.*, 2017, **27**, 1606750.
57 E. S. Parrott, R. L. Milot, T. Stergiopoulos, H. J. Snaith, M. B. Johnston and L. M. Herz, *J. Phys. Chem. Lett.*, 2016, **7**, 1321–1326.
58 N. Droseros, D. Tsokkou and N. Banerji, *Adv. Energy Mater.*, 2020, **10**, 1903258.
59 Q. Shang, Y. Wang, Y. Zhong, Y. Mi, L. Qin, Y. Zhao, X. Qiu, X. Liu and Q. Zhang, *J. Phys. Chem. Lett.*, 2017, **8**, 4431–4438.
60 M. B. Johnston and L. M. Herz, *Acc. Chem. Res.*, 2016, **49**, 146–154.
61 D. Luo, R. Su, W. Zhang, Q. Gong and R. Zhu, *Nat. Rev. Mater.*, 2020, **5**, 44–60.
62 B. Zhao, S. Bai, V. Kim, R. Lamboll, R. Shivanna, F. Auras, J. M. Richter, L. Yang, L. Dai, M. Alsari, X. J. She, L. Liang, J. Zhang, S. Lilliu, P. Gao, H. J. Snaith, J. Wang, N. C. Greenham, R. H. Friend and D. Di, *Nat. Photon.*, 2018, **12**, 783–789.
63 W. Deng, X. Jin, Y. Lv, X. Zhang, X. Zhang and J. Jie, *Adv. Funct. Mater.*, 2019, **29**, 1903861.
64 B. Yang and K. Han, *Acc. Chem. Res.*, 2019, **52**, 3188–3198.
65 G. Xing, B. Wu, X. Wu, M. Li, B. Du, Q. Wei, J. Guo, E. K. Yeow, T. C. Sum and W. Huang, *Nat. Commun.*, 2017, **8**, 1–9.

66 F. Zhang, B. Cai, J. Song, B. Han, B. Zhang and H. Zeng, *Adv. Funct. Mater.*, 2020, **30**, 2001732.
67 N. Droseros, G. Longo, J. C. Brauer, M. Sessolo, H. J. Bolink and N. Banerji, *ACS Energy Lett.*, 2018, **3**, 1458–1466.
68 F. Yang, H. Chen, R. Zhang, X. Liu, W. Zhang, J. Zhang, F. Gao and L. Wang, *Adv. Funct. Mater.*, 2020, **30**, 1908760.
69 Y. Tong, E. Bladt, M. F. Aygüler, A. Manzi, K. Z. Milowska, V. A. Hintermayr, P. Docampo, S. Bals, A. S. Urban and L. Polavarapu, *Angew. Chem., Int. Ed.*, 2016, **55**, 13887–13892.
70 X. Li, Y. Wu, S. Zhang, B. Cai, Y. Gu, J. Song and H. Zeng, *Adv. Funct. Mater.*, 2016, **26**, 2435–2445.
71 N. S. Makarov, S. Guo, O. Isaienko, W. Liu, I. Robel and V. I. Klimov, *Nano Lett.*, 2016, **16**, 2349–2362.
72 J. Lu, W. Feng, G. Mei, J. Sun, C. Yan, D. Zhang, K. Lin, D. Wu, K. Wang and Z. Wei, *Adv. Sci.*, 2020, **7**, 2000689.
73 W. Tress, *Adv. Energy Mater.*, 2017, **7**, 1602358.
74 X. Chen, H. Lu, Z. Li, Y. Zhai, P. F. Ndione, J. J. Berry, K. Zhu, Y. Yang and M. C. Beard, *ACS Energy Lett.*, 2018, **3**, 2273–2279.
75 Y. Jiang, C. Qin, M. Cui, T. He, K. Liu, Y. Huang, M. Luo, L. Zhang, H. Xu, S. Li, J. Wei, Z. Liu, H. Wang, G. H. Kim, M. Yuan and J. Chen, *Nat. Commun.*, 2019, **10**, 1868.
76 J. Aneesh, A. Swarnkar, V. Kumar Ravi, R. Sharma, A. Nag and K. V. Adarsh, *J. Phys. Chem. C*, 2017, **121**, 4734–4739.
77 V. I. Klimov, *Annu. Rev. Phys. Chem.*, 2007, **58**, 635–673.
78 M. Yuan, L. N. Quan, R. Comin, G. Walters, R. Sabatini, O. Voznyy, S. Hoogland, Y. Zhao, E. M. Beauregard and P. Kanjanaboos, *Nat. Nanotechnol.*, 2016, **11**, 872–877.
79 Y. Shang, Y. Liao, Q. Wei, Z. Wang, B. Xiang, Y. Ke, W. Liu and Z. Ning, *Sci. Adv.*, 2019, **5**, 1–9.
80 C. S. Ponseca Jr and V. Sundström, *Nanoscale*, 2016, **8**, 6249–6257.
81 E. M. Hutter, G. E. Eperon, S. D. Stranks and T. J. Savenije, *J. Phys. Chem. Lett.*, 2015, **6**, 3082–3090.
82 Y. Tian, A. Merdasa, M. Peter, M. Abdellah, K. Zheng, C. S. Ponseca Jr, T. N. Pullerits, A. Yartsev, V. Sundström and I. G. Scheblykin, *Nano Lett.*, 2015, **15**, 1603–1608.
83 S. Lee, J. H. Park, B. R. Lee, E. D. Jung, J. C. Yu, D. Di Nuzzo, R. H. Friend and M. H. Song, *J. Phys. Chem. Lett.*, 2017, **8**, 1784–1792.
84 T. Tachikawa, I. Karimata and Y. Kobori, *J. Phys. Chem. Lett.*, 2015, **6**, 3195–3201.
85 F. Hu, H. Zhang, C. Sun, C. Yin, B. Lv, C. Zhang, W. W. Yu, X. Wang, Y. Zhang and M. Xiao, *ACS Nano*, 2015, **9**, 12410–12416.
86 O. Ostroverkhova, *Handbook of Organic Materials for Electronic and Photonic Devices*, Woodhead Publishing, 2018.
87 P. Teng, S. Reichert, W. Xu, S. C. Yang, F. Fu, Y. Zou, C. Yin, C. Bao, M. Karlsson, X. Liu, J. Qin, T. Yu, W. Tress, Y. Yang, B. Sun, C. Deibel and F. Gao, *Matter*, 2021, **4**, 3710–3724.
88 Q. Shen, Y. Hao, L. Ma and X. Wang, *J. Phys. Chem. Lett.*, 2021, **12**, 7019–7025.
89 C. Wang, D. Han, J. Wang, Y. Yang, X. Liu, S. Huang, X. Zhang, S. Chang, K. Wu and H. Zhong, *Nat. Commun.*, 2020, **11**, 1–8.
90 H. Cho, C. Wolf, J. S. Kim, H. J. Yun, J. S. Bae, H. Kim, J. M. Heo, S. Ahn and T. W. Lee, *Adv. Mater.*, 2017, **29**, 1700579.
91 Y. Ling, Y. Tian, X. Wang, J. C. Wang, J. M. Knox, F. Perez-Orive, Y. Du, L. Tan, K. Hanson, B. Ma and H. Gao, *Adv. Mater.*, 2016, **28**, 8983–8989.
92 C. Wu, Y. Zou, T. Wu, M. Ban, V. Pecunia, Y. Han, Q. Liu, T. Song, S. Duhm and B. Sun, *Adv. Funct. Mater.*, 2017, **27**, 1700338.
93 V. I. Klimov, A. A. Mikhailovsky, D. W. McBranch, C. A. Leatherdale and M. G. Bawendi, *Science*, 2000, **287**, 1011–1013.
94 J. A. McGuire, J. Joo, J. M. Pietryga, R. D. Schaller and V. I. Klimov, *Acc. Chem. Res.*, 2008, **41**, 1810–1819.
95 C. Sun, Y. Jiang, M. Cui, L. Qiao, J. Wei, Y. Huang, L. Zhang, T. He, S. Li, H. Y. Hsu, C. Qin, R. Long and M. Yuan, *Nat. Commun.*, 2021, **12**, 2207.
96 T. Ishihara, J. Takahashi and T. Goto, *Phy. Rev. B*, 1990, **42**, 11099–11107.
97 P. Pang, G. Jin, C. Liang, B. Wang, W. Xiang, D. Zhang, J. Xu, W. Hong, Z. Xiao and L. Wang, *ACS Nano*, 2020, **14**, 11420–11430.
98 M. Kumagai and T. Takagahara, *Phy. Rev. B*, 1989, **40**, 12359.
99 M. D. Smith, L. Pedesseau, M. Kepenekian, I. C. Smith, C. Katan, J. Even and H. I. Karunadasa, *Chem. Sci.*, 2017, **8**, 1960–1968.
100 D. Ma, K. Lin, Y. Dong, H. Choubisa, A. H. Proppe, D. Wu, Y. K. Wang, B. Chen, P. Li, J. Z. Fan, F. Yuan, A. Johnston, Y. Liu, Y. Kang, Z. H. Lu, Z. Wei and E. H. Sargent, *Nature*, 2021, **599**, 594–598.
101 Z. Ren, J. Yu, Z. Qin, J. Wang, J. Sun, C. C. Chan, S. Ding, K. Wang, R. Chen and K. S. Wong, *Adv. Mater.*, 2021, **33**, 2005570.
102 S. Ahmad, P. Fu, S. Yu, Q. Yang, X. Liu, X. Wang, X. Wang, X. Guo and C. Li, *Joule*, 2019, **3**, 794–806.
103 Y. Liu, B. Dong, A. Hagfeldt, J. Luo and M. Graetzel, *SmartMat*, 2021, **2**, 33–37.
104 Z. Chu, Y. Zhao, F. Ma, C. X. Zhang, H. Deng, F. Gao, Q. Ye, J. Meng, Z. Yin, X. Zhang and J. You, *Nat. Commun.*, 2020, **11**, 4165.
105 J. Zhang, X. Xing, D. Qian, A. Wang, L. Gu, Z. Kuang, J. Wang, H. Zhang, K. Wen, W. Xu, M. Niu, X. Du, L. Yuan, C. Cao, Y. Cao, L. Zhu, N. Wang, C. Yi, W. Huang and J. Wang, *Adv. Funct. Mater.*, 2022, 2111578.
106 D. Liang, Y. Peng, Y. Fu, M. J. Shearer, J. Zhang, J. Zhai, Y. Zhang, R. J. Hamers, T. L. Andrew and S. Jin, *ACS Nano*, 2016, **10**, 6897–6904.
107 M. Karlsson, Z. Yi, S. Reichert, X. Luo, W. Lin, Z. Zhang, C. Bao, R. Zhang, S. Bai, G. Zheng, P. Teng, L. Duan, Y. Lu, K. Zheng, T. Pullerits, C. Deibel, W. Xu, R. Friend and F. Gao, *Nat. Commun.*, 2021, **12**, 361.
108 F. Zhang, H. Zhong, C. Chen, X. G. Wu, X. Hu, H. Huang, J. Han, B. Zou and Y. Dong, *ACS Nano*, 2015, **9**, 4533–4542.
109 X. Zhu, L. Ge, Y. Wang, M. Li, R. Zhang, M. Xu, Z. Zhao, W. Lv and R. Chen, *Adv. Opt. Mater.*, 2021, **9**, 2100058.

110 L. Protesescu, S. Yakunin, M. I. Bodnarchuk, F. Krieg, R. Caputo, C. H. Hendon, R. X. Yang, A. Walsh and M. V. Kovalenko, *Nano Lett.*, 2015, **15**, 3692–3696.
111 P. Liu, W. Chen, W. Wang, B. Xu, D. Wu, J. Hao, W. Cao, F. Fang, Y. Li and Y. Zeng, *Chem. Mater.*, 2017, **29**, 5168–5173.
112 A. Dutta, R. K. Behera, P. Pal, S. Baitalik and N. Pradhan, *Angew. Chem., Int. Ed.*, 2019, **58**, 5552–5556.
113 S. Paul and A. Samanta, *ACS Energy Lett.*, 2020, **5**, 64–69.
114 M. Imran, V. Caligiuri, M. Wang, L. Goldoni, M. Prato, R. Krahne, L. De Trizio and L. Manna, *J. Am. Chem. Soc.*, 2018, **140**, 2656–2664.
115 S. Bera, R. K. Behera and N. Pradhan, *J. Am. Chem. Soc.*, 2020, **142**, 20865–20874.
116 N. Pradhan, *ACS Energy Lett.*, 2019, **4**, 1634–1638.
117 Y. Dong, T. Qiao, D. Kim, D. Parobek, D. Rossi and D. H. Son, *Nano Lett.*, 2018, **18**, 3716–3722.
118 Z. J. Yong, S. Q. Guo, J. P. Ma, J. Y. Zhang, Z. Y. Li, Y. M. Chen, B. B. Zhang, Y. Zhou, J. Shu, J. L. Gu, L. R. Zheng, O. M. Bakr and H. T. Sun, *J. Am. Chem. Soc.*, 2018, **140**, 9942–9951.
119 S. Das Adhikari, R. K. Behera, S. Bera and N. Pradhan, *J. Phys. Chem. Lett.*, 2019, **10**, 1530–1536.
120 N. Mondal, A. De and A. Samanta, *ACS Energy Lett.*, 2019, **4**, 32–39.
121 M. Imran, J. Ramade, F. Di Stasio, M. De Franco, J. Buha, S. Van Aert, L. Goldoni, S. Lauciello, M. Prato, I. Infante, S. Bals and L. Manna, *Chem. Mater.*, 2020, **32**, 10641–10652.
122 M. Zeng, F. Artizzu, J. Liu, S. Singh, F. Locardi, D. Mara, Z. Hens and R. V. Deun, *ACS Appl. Nano Mater.*, 2020, **3**, 4699–4707.
123 P. J. S. Rana, T. Swetha, H. Mandal, A. Saeki, P. R. Bangal and S. P. Singh, *J. Phys. Chem. C*, 2019, **123**, 17026–17034.
124 N. Mondal, A. De and A. Samanta, *J. Phys. Chem. Lett.*, 2018, **9**, 3673–3679.
125 F. Liu, Y. Zhang, C. Ding, S. Kobayashi, T. Izuishi, N. Nakazawa, T. Toyoda, T. Ohta, S. Hayase, T. Minemoto, K. Yoshino, S. Dai and Q. Shen, *ACS Nano*, 2017, **11**, 10373–10383.
126 Y. Shynkarenko, M. I. Bodnarchuk, C. Bernasconi, Y. Berezovska, V. Verteletskyi, S. T. Ochsenbein and M. V. Kovalenko, *ACS Energy Lett.*, 2019, **4**, 2703–2711.
127 H. Sun, Z. Yang, M. Wei, W. Sun, X. Li, S. Ye, Y. Zhao, H. Tan, E. L. Kynaston and T. B. Schon, *Adv. Mater.*, 2017, **29**, 1701153.
128 J. Leng, T. Wang, X. Zhao, E. W. Y. Ong, B. Zhu, J. D. A. Ng, Y. C. Wong, K. H. Khoo, K. Tamada and Z. K. Tan, *J. Phys. Chem. Lett.*, 2020, **11**, 2036–2043.
129 A. Dutta, R. K. Behera, S. K. Dutta, S. Das Adhikari and N. Pradhan, *J. Phys. Chem. Lett.*, 2018, **9**, 6599–6604.
130 A. Dutta, S. K. Dutta, S. Das Adhikari and N. Pradhan, *ACS Energy Lett.*, 2018, **3**, 329–334.
131 C. Luo, C. Yan, W. Li, F. Chun, M. Xie, Z. Zhu, Y. Gao, B. Guo and W. Yang, *Adv. Funct. Mater.*, 2020, **30**, 2000026.
132 G. Almeida, I. Infante and L. Manna, *Science*, 2019, **364**, 833–834.
133 J. Li, L. Xu, T. Wang, J. Song, J. Chen, J. Xue, Y. Dong, B. Cai, Q. Shan and B. Han, *Adv. Mater.*, 2017, **29**, 1603885.
134 Y. Zhang, T. D. Siegler, C. J. Thomas, M. K. Abney, T. Shah, A. De Gorostiza, R. M. Greene and B. A. Korgel, *Chem. Mater.*, 2020, **32**, 5410–5423.
135 S. ten Brinck, F. Zaccaria and I. Infante, *ACS Energy Lett.*, 2019, **4**, 2739–2747.
136 J. Liu, K. Song, Y. Shin, X. Liu, J. Chen, K. X. Yao, J. Pan, C. Yang, J. Yin, L. J. Xu, H. Yang, A. M. El-Zohry, B. Xin, S. Mitra, M. N. Hedhili, I. S. Roqan, O. F. Mohammed, Y. Han and O. M. Bakr, *Chem. Mater.*, 2019, **31**, 6642–6649.
137 Y. Bai, M. Hao, S. Ding, P. Chen and L. Wang, *Adv. Mater.*, 2021, 2105958.
138 D. P. Nenon, K. Pressler, J. Kang, B. A. Koscher, J. H. Olshansky, W. T. Osowiecki, M. A. Koc, L. W. Wang and A. P. Alivisatos, *J. Am. Chem. Soc.*, 2018, **140**, 17760–17772.
139 M. I. Bodnarchuk, S. C. Boehme, S. ten Brinck, C. Bernasconi, Y. Shynkarenko, F. Krieg, R. Widmer, B. Aeschlimann, D. Günther, M. V. Kovalenko and I. Infante, *ACS Energy Lett.*, 2019, **4**, 63–74.
140 F. Staub, U. Rau and T. Kirchartz, *ACS Omega*, 2018, **3**, 8009–8016.
141 S. Nakahara, H. Tahara, G. Yumoto, T. Kawawaki, M. Saruyama, R. Sato, T. Teranishi and Y. Kanemitsu, *J. Phys. Chem. C*, 2018, **122**, 22188–22193.
142 X. Zheng, Y. Hou, H. T. Sun, O. F. Mohammed, E. H. Sargent and O. M. Bakr, *J. Phys. Chem. Lett.*, 2019, **10**, 2629–2640.
143 J. Shamsi, D. Kubicki, M. Anaya, Y. Liu, K. Ji, K. Frohna, C. P. Grey, R. H. Friend and S. D. Stranks, *ACS Energy Lett.*, 2020, **5**, 1900–1907.
144 X. Min, Q. Xie, Z. Wang, X. Wang and M. Chen, *Mater. Chem. Phys.*, 2022, **276**, 125404.
145 Q. Zhong, J. Liu, S. Chen, P. Li, J. Chen, W. Guan, Y. Qiu, Y. Xu, M. Cao and Q. Zhang, *Adv. Opt. Mater.*, 2021, **9**, 2001763.
146 B. A. Koscher, Z. Nett and A. P. Alivisatos, *ACS Nano*, 2019, **13**, 11825–11833.
147 Q. Jing, M. Zhang, X. Huang, X. Ren, P. Wang and Z. Lu, *Nanoscale*, 2017, **9**, 7391–7396.
148 C. Zou, Y. Liu, D. S. Ginger and L. Y. Lin, *ACS Nano*, 2020, **14**, 6076–6086.
149 Y. Liu, T. Wu, Y. Liu, T. Song and B. Sun, *APL Mater.*, 2019, **7**, 021102.
150 P. Lu, J. Wu, X. Shen, X. Gao, Z. Shi, M. Lu, W. W. Yu and Y. Zhang, *Adv. Sci.*, 2020, **7**, 2001562.
151 Y. Wang, Y. Teng, P. Lu, X. Shen, P. Jia, M. Lu, Z. Shi, B. Dong, W. W. Yu and Y. Zhang, *Adv. Funct. Mater.*, 2020, **30**, 1910140.
152 Z. Li, Z. Chen, Y. Yang, Q. Xue, H. L. Yip and Y. Cao, *Nat. Commun.*, 2019, **10**, 1027.
153 P. Chen, Z. Xiong, X. Wu, M. Shao, X. Ma, Z. H. Xiong and C. Gao, *J. Phys. Chem. Lett.*, 2017, **8**, 1810–1818.
154 S. Yuan, B. Han, T. Fang, Q. Shan and J. Song, *ACS Appl. Electron. Mater.*, 2020, **2**, 3530–3537.

155 M. Guo, Y. Lu, X. Y. Cai, Y. Shen, X. Y. Qian, H. Ren, Y. Li, W. Wang and J. Tang, *J. Mater. Chem. C*, 2022, **10**, 2998–3005.
156 S. Ahn, M. H. Park, S. H. Jeong, Y. H. Kim, J. Park, S. Kim, H. Kim, H. Cho, C. Wolf and M. Pei, *Adv. Funct. Mater.*, 2019, **29**, 1807535.
157 R. Fan, L. Song, Y. Hu, X. Guo, X. Liu, L. Wang, C. Geng, S. Xu, Y. Zhang, Z. Zhang, N. Luan and W. Bi, *ACS Appl. Mater. Interfaces*, 2020, **12**, 43331–43338.
158 X. Huang, R. Bäuerle, F. Scherz, J. N. Tisserant, W. Kowalsky, R. Lovrinčić and G. Hernandez-Sosa, *J. Mater. Chem. C*, 2021, **9**, 4344–4350.
159 M. Abdi-Jalebi, Z. Andaji-Garmaroudi, S. Cacovich, C. Stavrakas, B. Philippe, J. M. Richter, M. Alsari, E. P. Booker, E. M. Hutter, A. J. Pearson, S. Lilliu, T. J. Savenije, H. Rensmo, G. Divitini, C. Ducati, R. H. Friend and S. D. Stranks, *Nature*, 2018, **555**, 497–501.
160 R. Lai and K. Wu, *J. Chem. Phys.*, 2019, **151**, 194701.
161 J. Piprek, *Phys. Status Solidi A*, 2010, **207**, 2217–2225.
162 Z. Guo, Y. Zhang, B. Wang, L. Wang, N. Zhou, Z. Qiu, N. Li, Y. Chen, C. Zhu and H. Xie, *Adv. Mater.*, 2021, **33**, 2102246.
163 N. Li, L. Song, Y. Jia, Y. Dong, F. Xie, L. Wang, S. Tao and N. Zhao, *Adv. Mater.*, 2020, **32**, 1907786.
164 L. Zhang, F. Yuan, J. Xi, B. Jiao, H. Dong, J. Li and Z. Wu, *Adv. Funct. Mater.*, 2020, **30**, 2001834.
165 M. Xu, Q. Peng, W. Zou, L. Gu, L. Xu, L. Cheng, Y. He, M. Yang, N. Wang and W. Huang, *Appl. Phys. Lett.*, 2019, **115**, 041102.